




ARTICLE

CLASPs stabilize the pre-catastrophe intermediate state between microtubule growth and shrinkage

Elizabeth J. Lawrence¹, Saptarshi Chatterjee¹, and Marija Zanic^{1,2,3}

Cytoplasmic linker-associated proteins (CLASPs) regulate microtubules in fundamental cellular processes. CLASPs stabilize dynamic microtubules by suppressing microtubule catastrophe and promoting rescue, the switch-like transitions between growth and shrinkage. How CLASPs specifically modulate microtubule transitions is not understood. Here, we investigate the effects of CLASPs on the pre-catastrophe intermediate state of microtubule dynamics, employing distinct microtubule substrates to mimic the intermediate state. Surprisingly, we find that CLASP1 promotes the depolymerization of stabilized microtubules in the presence of GTP, but not in the absence of nucleotide. This activity is also observed for CLASP2 family members and a minimal TOG2-domain construct. Conversely, we find that CLASP1 stabilizes unstable microtubules upon tubulin dilution in the presence of GTP. Strikingly, our results reveal that CLASP1 drives microtubule substrates with vastly different inherent stabilities into the same slowly depolymerizing state in a nucleotide-dependent manner. We interpret this state as the pre-catastrophe intermediate state. Therefore, we conclude that CLASPs suppress microtubule catastrophe by stabilizing the intermediate state between growth and shrinkage.

Introduction

Microtubules are dynamic cytoskeletal polymers essential for many fundamental cellular processes. Individual microtubules undergo dynamic instability, switching between phases of growth and shrinkage through transitions known as catastrophe and rescue (Mitchison and Kirschner, 1984). To facilitate their roles in diverse cellular processes, microtubules are regulated by a large number of microtubule-associated proteins (MAPs). Cytoplasmic linker-associated proteins (CLASPs) are a highly conserved family of MAPs that stabilize microtubules in many cellular contexts including cell division, cell migration, and neuronal development (Lawrence et al., 2020; Akhmanova et al., 2001). Human CLASPs stabilize microtubules by autonomously suppressing microtubule catastrophe and promoting microtubule rescue without changing the rates of microtubule growth or shrinkage (Aher et al., 2018; Lawrence and Zanic, 2019; Lawrence et al., 2018). However, the molecular mechanisms underlying CLASP's activity remain largely unknown.

CLASPs belong to a larger group of proteins that use tubulin-binding tumor overexpression gene (TOG) domains to modulate microtubule dynamics (Al-Bassam and Chang, 2011; Slep, 2009; Farmer and Zanic, 2021). Humans possess two CLASP paralogs: CLASP1 and CLASP2, with multiple TOG domains contained within all major isoforms (CLASP1 α , CLASP2 α , and CLASP2 γ).

While CLASPs contain multiple TOG domains, the isolated TOG2 domain from both yeast and mammalian homologues is sufficient for the microtubule regulatory activity of the full-length protein (Aher et al., 2018; Majumdar et al., 2018; Funk et al., 2014). Previous work established that a minimal construct containing a single TOG2 domain of human CLASP2 α recapitulates the anti-catastrophe and rescue activity of full-length human CLASP2 α on dynamically growing microtubules (Aher et al., 2018). Interestingly, this TOG domain was reported to adopt a uniquely curved architecture, not compatible with binding to known tubulin dimer conformations (Lawrence et al., 2020; Leano et al., 2013; Leano and Slep, 2019; Maki et al., 2015). This unique TOG2 architecture may thus underlie CLASPs ability to specifically regulate the transitions between microtubule growth and shrinkage.

Interestingly, an early model of microtubule dynamic instability proposed the existence of a metastable intermediate state between the microtubule growth and shrinkage phases (Tran et al., 1997; Janosi et al., 2002). This model is supported by observations that growing microtubules exhibit a brief delay prior to the onset of catastrophe upon the removal of tubulin in solution (Walker et al., 1991; Duellberg et al., 2016; Voter et al., 1991; Strothman et al., 2019). Furthermore, recent high-temporal

¹Department of Cell and Developmental Biology, Vanderbilt University, Nashville, TN, USA; ²Department of Chemical and Biomolecular Engineering, Vanderbilt University, Nashville, TN, USA; ³Department of Biochemistry, Vanderbilt University, Nashville, TN, USA.

Correspondence to Elizabeth J. Lawrence: beth.lawrence@vanderbilt.edu; Marija Zanic: marija.zanic@vanderbilt.edu.

© 2023 Lawrence et al. This article is distributed under the terms of an Attribution–Noncommercial–Share Alike–No Mirror Sites license for the first six months after the publication date (see <http://www.rupress.org/terms/>). After six months it is available under a Creative Commons License (Attribution–Noncommercial–Share Alike 4.0 International license, as described at <https://creativecommons.org/licenses/by-nc-sa/4.0/>).

resolution measurements of dynamic microtubule growth found that microtubules exhibit a distinct slowdown in growth prior to catastrophe (Maurer et al., 2014; Mahserejian et al., 2022; Farmer et al., 2021). Importantly, in the presence of CLASP, microtubules can withstand large growth fluctuations, and return to a robust growth phase following transient growth slowdowns, thus avoiding catastrophe (Lawrence et al., 2018; Mahserejian et al., 2022). Furthermore, CLASPs promote microtubule pausing in cells and in vitro, and stabilize microtubule ends at anchor points such as kinetochores, focal adhesions, and the cell cortex (Mahserejian et al., 2022; Li et al., 2012; Sousa et al., 2007; Aher et al., 2018; Lawrence et al., 2020). Therefore, we hypothesize that CLASPs stabilize microtubules in the pre-catastrophe state, an intermediate state between microtubule growth and shrinkage. Here, we investigate the effects of CLASPs on distinct microtubule substrates to unravel the molecular mechanisms by which CLASPs regulate microtubule catastrophe and rescue.

Results

CLASP1 promotes the depolymerization of stabilized microtubules in a nucleotide-dependent manner

To determine the effect of CLASP on distinct microtubule end conformations, we first investigated CLASP1's activity on stabilized microtubules in the absence of tubulin. Another prominent TOG-domain protein, microtubule polymerase XMAP215, uses its TOG domains to induce the depolymerization of microtubules in the absence of tubulin by promoting a weakly bound state of tubulin at the microtubule end (Brouhard et al., 2008). Stabilization of a weakly bound tubulin dimer explains both XMAP215's potent microtubule polymerase activity in the presence and depolymerase activity in the absence of soluble tubulin, establishing XMAP215's mechanism of microtubule regulation. To investigate whether CLASP1, like XMAP215, has the ability to depolymerize stabilized microtubules, we used an established in vitro assay, combining TIRF microscopy with purified protein components (Fig. 1 A; Gell et al., 2010). Briefly, stable microtubules were polymerized with GMPCPP (guanosine-5'-[(α,β)-methylene]triphosphate), a slowly hydrolyzable GTP analog, and adhered to coverslips. Microtubule depolymerization was monitored over 15 min under different reaction conditions. In the buffer control condition, in the absence of any MAPs, microtubules depolymerized very slowly over the course of the experiment, as expected (Fig. 1 B left, Fig. 1 D; 0.29 ± 0.04 nm/s; SE, $N = 90$). As a positive control, we purified recombinant chTOG (Fig. S1), the human homolog of XMAP215, and tested its depolymerase activity. Indeed, we observed microtubule depolymerization with 200 nM chTOG (Fig. 1 B middle; 2.64 ± 0.02 nm/s; SE, $N = 50$, $P < 0.001$ compared to the buffer control). Thus, like XMAP215, human chTOG induces microtubule depolymerization in the absence of soluble tubulin. In contrast, when stabilized microtubules were incubated with 200 nM purified recombinant CLASP1 (Fig. S1), we did not observe significant microtubule depolymerization (Fig. 1 B right; 0.248 ± 0.008 nm/s; SE, $N = 79$; $P > 0.05$ compared to the buffer control). Thus, unlike XMAP215/chTOG, CLASP1 does not promote microtubule depolymerization under these conditions.

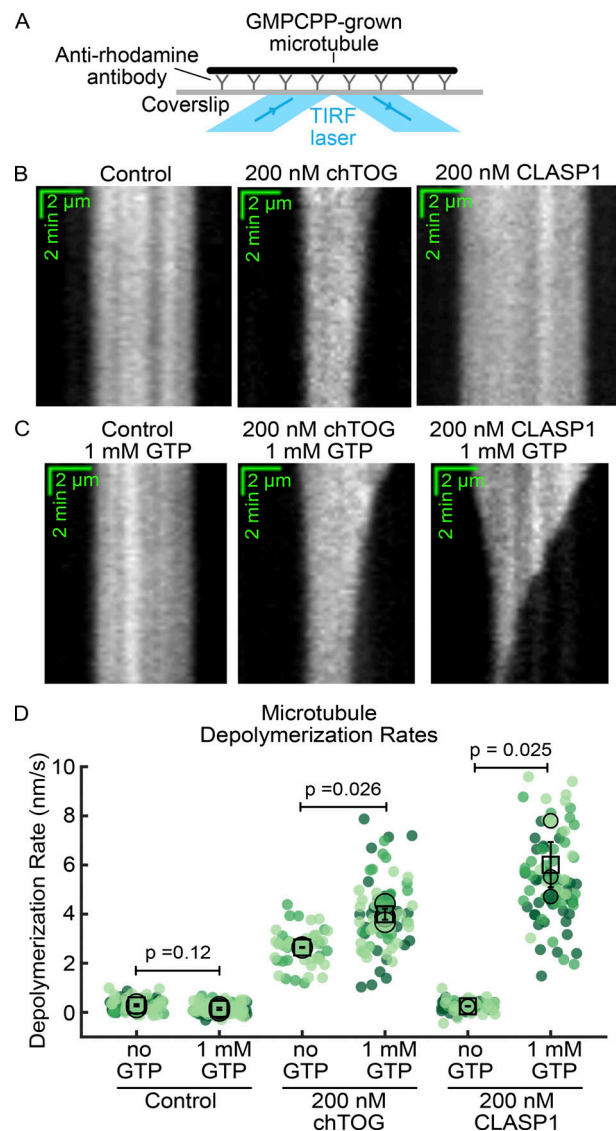


Figure 1. CLASP1 promotes the depolymerization of GMPCPP-stabilized microtubules in a GTP-dependent manner. (A) Schematic of the microtubule depolymerization assay. (B) Representative kymographs of GMPCPP-stabilized microtubules incubated with storage buffer, 200 nM chTOG, or 200 nM CLASP1. (C) Representative kymographs of GMPCPP-stabilized microtubules incubated with storage buffer, 200 nM chTOG, or 200 nM CLASP1 in the presence of 1 mM GTP. (D) Quantification of microtubule depolymerization rates for the conditions in B and C. $N = 50$ –108 microtubules for each condition across at least two experimental days. Individual data points from different experiments are plotted in different shades, and the means for each experimental repeat are plotted as larger points in the same color. The squares indicate the average of the experimental means, and the vertical bars are the standard errors of the means. See also Video 1. For comparison between the no GTP conditions, a one-way ANOVA followed by Tukey's HSD test for multiple comparisons found that the mean rate of microtubule depolymerization was significantly different between the buffer control vs. chTOG ($P < 0.001$) and chTOG vs. CLASP1 ($P < 0.001$) in the absence of GTP. There was no statistically significant difference between the buffer control and CLASP1 condition ($P = 0.06$) in the absence of GTP. Welch's two-tailed unequal variances t tests were performed for pairwise comparison of the no-GTP vs. GTP conditions and the corresponding P values are indicated on the graph.

The configuration of microtubule ends depends on the nucleotide state of the end-bound tubulin dimers (Brouhard and Rice, 2014; Gudimchuk and McIntosh, 2021). Given that the

specific configuration of tubulin recognized by CLASP's TOG domains is not known, we wondered whether CLASP1's activity is sensitive to the nucleotide state of the tubulin at the microtubule ends. Therefore, we investigated the effects of including GTP in the reaction mixture for our depolymerization assay, which is expected to exchange with the GMPCPP bound to the terminal tubulin dimers (Mitchison, 1993; Fig. 1 B). The addition of 1 mM GTP to the buffer control condition did not promote microtubule depolymerization on its own (Fig. 1 B left, Fig. 1 C; 0.14 ± 0.05 nm/s; SE, $N = 108$; $P = 0.25$ compared to the no GTP control). Furthermore, chTOG displayed only a mild, 1.5-fold increase in depolymerase activity in the presence of 1 mM GTP compared to the no GTP condition (Fig. 1 B middle, Fig. 1 C; 4.0 ± 0.2 nm/s; SE, $N = 77$). In contrast, upon introduction of 200 nM CLASP1 and 1 mM GTP, the microtubules robustly depolymerized, displaying a 24-fold increase in depolymerization rate when compared to CLASP1 without GTP (Fig. 1 B right, Fig. 1 C and Video 1; 6.0 ± 0.9 nm/s; SE, $N = 89$; $P = 0.025$ compared to CLASP1 without GTP). These results demonstrate that, in the absence of soluble tubulin, CLASP1 promotes microtubule depolymerization in a GTP-dependent manner.

Since we observed GTP-dependent CLASP activity, we next investigated the specific effects of different nucleotides. We performed sequential nucleotide exchange experiments in which the CLASP1 concentration was maintained constant but the solution was exchanged for reaction mixtures containing distinct nucleotides (Fig. S2). First, we incubated microtubules in the presence of CLASP1 without any nucleotide in the solution, and saw no depolymerization, as expected. Next, we introduced 1 mM GTP in the same observation channel and observed depolymerization. Finally, we exchanged the reaction solution to include 1 mM GMPCPP and found that depolymerization quickly stopped (Fig. S2 A). Thus, microtubule depolymerization is switched on with GTP and switched off with GMPCPP in the presence of CLASP1. To determine whether GTP hydrolysis is necessary for CLASP-mediated microtubule depolymerization, we investigated CLASP1 activity in the presence of post-hydrolysis nucleotides GDP and GTP γ S (guanosine 5'-O-[gamma-thio]triphosphate), a nucleotide analog that mimics the GDP-Pi state (Fig. S2, B and C). Surprisingly, microtubules robustly depolymerized in the presence of CLASP1 with 1 mM GDP. Furthermore, in the presence of CLASP1 with 1 mM GTP γ S, a slow but significant rate of microtubule depolymerization was observed ($P < 0.001$ for the GTP γ S versus GMPCPP conditions). Taken together these data demonstrate that the post-hydrolysis state of GTP facilitates CLASP-mediated microtubule depolymerization, but that GTP hydrolysis itself is not strictly required. Our results suggest that CLASP recognizes a nucleotide-dependent configuration of the microtubule end, which may underlie CLASP's anti-catastrophe activity.

CLASP1 stabilizes unstable microtubule ends in the absence of soluble tubulin in a nucleotide-dependent manner

In physiological conditions, CLASPs operate along with tubulin in solution and stabilize dynamic microtubules by specifically suppressing catastrophe and promoting rescue (Aher et al., 2018; Lawrence et al., 2018; Lawrence and Zanic, 2019). In the case of

the polymerase XMAP215, the addition of stoichiometric amounts of soluble tubulin (100 nM) abolishes its microtubule depolymerase activity (Brouhard et al., 2008). We wondered if similar suppression of microtubule depolymerization would be observed with CLASP1 and soluble tubulin. Surprisingly, we found that addition of 1 μ M tubulin to 200 nM CLASP1 did not abolish CLASP1-mediated microtubule depolymerization (Fig. S3). Titrating the soluble tubulin concentration revealed that the depolymerization activity was not abolished until tubulin concentrations reached 6 μ M, at which point persistent microtubule polymerization was observed. Thus, when the microtubule end switches to a growth phase at concentrations above the critical concentration for templated microtubule nucleation, CLASP1 no longer promotes microtubule depolymerization but rather stabilizes microtubule growth. Interestingly, we observed instances of simultaneous CLASP1-mediated depolymerization at one microtubule end and stabilization of growth at the other end at a concentration of tubulin as high as 8 μ M tubulin (Fig. S3 C). Based on these observations, we conclude that CLASP1's activity is likely regulated by a specific configuration of the microtubule end.

To determine whether CLASP's anti-catastrophe activity requires tubulin in solution, we performed "tubulin dilution" experiments with unstable microtubule lattices. It has been previously observed that microtubules exhibit a brief phase of slow depolymerization prior to catastrophe upon tubulin dilution (Duellberg et al., 2016). This phase is thought to correspond to an intermediate state in which the microtubule end contains a mixture of both GTP- and GDP-bound tubulin dimers. First, we polymerized microtubules using a mixture of GTP and GMPCPP to mimic microtubule ends in a pre-catastrophe state (Fig. 2 A, see Materials and methods). When soluble tubulin was subsequently diluted, the mixed-nucleotide microtubules slowly depolymerized. The rates of slow depolymerization were similar regardless of the nucleotide in solution (Fig. 2, A and C, "mixed-nucleotide lattice" control conditions). Contrary to our observations on stable microtubules, with the addition of 20 nM CLASP1 and either 1 mM GTP or 1 mM GDP, microtubule depolymerization rates did not accelerate, and the microtubules were maintained in a prolonged slowly depolymerizing state (Fig. 2, A and C). Strikingly, when CLASP1 and GMPCPP were introduced to the unstable mixed-nucleotide lattice, we found that the microtubules were completely stabilized, with a mean depolymerization rate of 0.33 ± 0.04 nm/s (SE, $N = 26$) for the CLASP1 condition vs. 16.8 ± 0.7 nm/s (SE, $N = 30$) for GMPCPP-only condition (Fig. 2, A and C; $P = 0.002$). Therefore, while GMPCPP on its own is not sufficient to stabilize unstable microtubules, CLASP1 in the presence of GMPCPP is able to completely prevent microtubule depolymerization, even in the absence of soluble tubulin.

Next, we induced the pre-catastrophe state on dynamic microtubules. To achieve this, we performed tubulin dilution experiments on dynamic microtubules polymerized with GTP. We exchanged the polymerization mixture for a reaction solution containing different nucleotides, alone or with CLASP1 (Fig. 2 B). Upon dilution of soluble tubulin with any of the nucleotides alone, the microtubules underwent catastrophe within a few

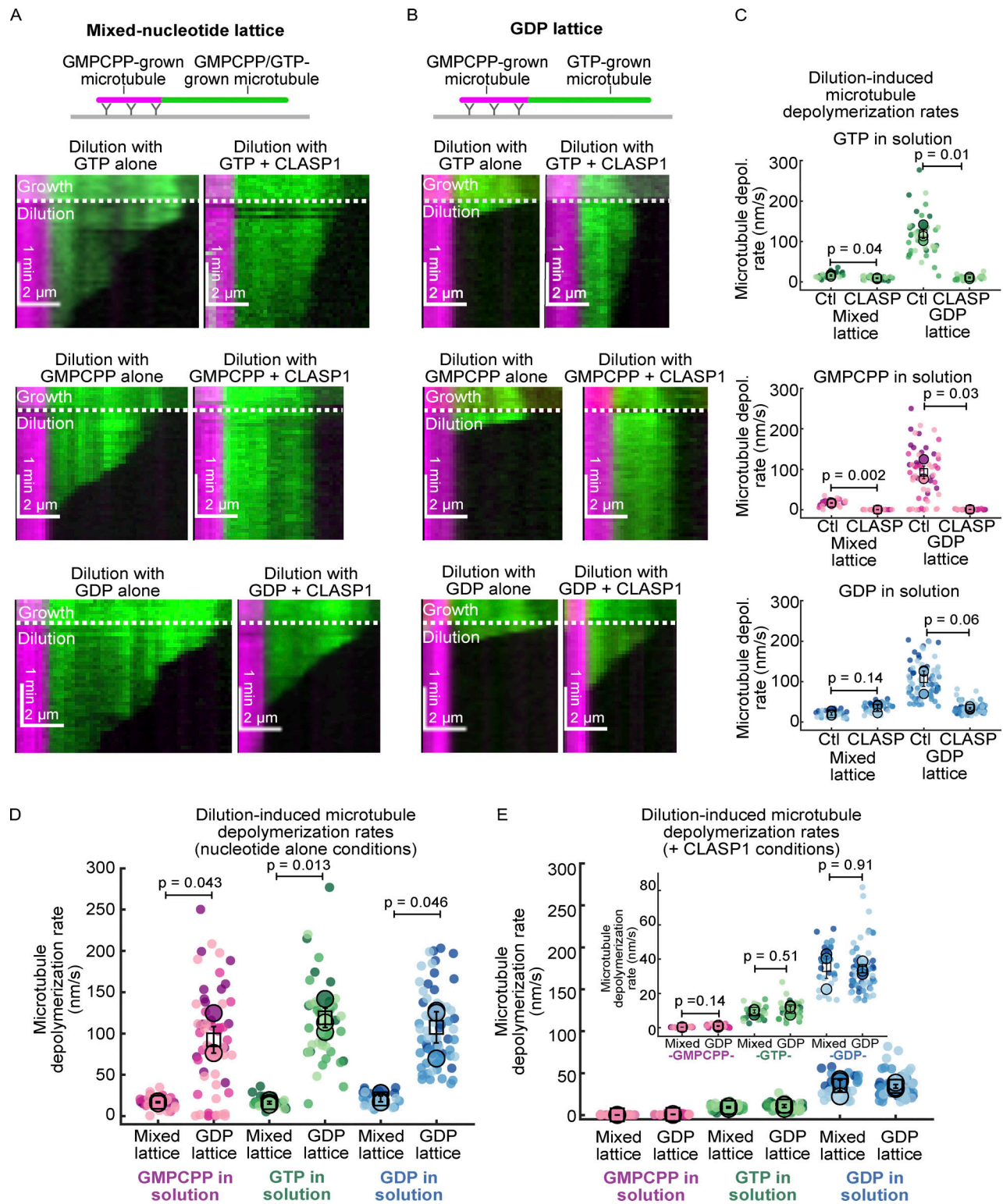


Figure 2. **CLASP1 stabilizes unstable microtubule ends in a nucleotide-dependent manner.** (A) Representative kymographs of mixed-nucleotide microtubule extensions (green) undergoing depolymerization after tubulin dilution. Microtubules were grown with 7 μ M A488 tubulin, 0.8 mM GMPCPP, and 0.2 mM GTP, and then the buffer was exchanged while imaging (dotted white line) for nucleotides alone or in the presence of 20 nM CLASP1. (B) Representative kymographs of GDP microtubule extensions (green) undergoing depolymerization after tubulin dilution. Microtubules were first grown with 12 μ M A488 tubulin and 100 μ M GTP, and then the buffer was exchanged while imaging (dotted white line) for nucleotides alone or in the presence of 20 nM CLASP1. (C) Quantification of the mixed-lattice and GDP-lattice microtubule depolymerization rates following dilution with and without CLASP1 in the presence of different nucleotides. $N = 25$ –64 microtubules for each condition obtained across three experimental days. Individual data points from different experiments are plotted in different shades. The means for each experimental repeat are plotted as larger points in the same color. The squares indicate the average of the experimental means and the vertical bars are the standard errors of the means. The mean rates and statistics can be found in Table S1. (C–E) The data in C

were replotted to show dilution-induced microtubule depolymerization rates in the presence of nucleotides alone (D) and in the presence of CLASP (E) for the different microtubule templates. Welch's two-tailed unequal variances *t* tests were performed, and the corresponding *P* values are indicated on the graphs.

seconds, characterized by the onset of fast depolymerization, as expected (Duellberg et al., 2016; Walker et al., 1991; Strothman et al., 2019; Voter et al., 1991; Fig. 2, B and C, "GDP-lattice" control conditions). In contrast, upon dilution with CLASP1 and GTP, the microtubules were maintained in the slow shrinkage phase, depolymerizing an order of magnitude slower than the control (Fig. 2, B and C). Dilution with CLASP1 and GDP resulted in more moderate microtubule stabilization. Furthermore, when the growth mixture was exchanged for CLASP1 and GMPCPP, the microtubules did not undergo catastrophe and remained stable. Taken together, our results demonstrate that CLASP1's anti-catastrophe activity is nucleotide-dependent but does not require soluble tubulin.

Strikingly, we noticed that the depolymerization rates of the different microtubule substrates were remarkably similar in the presence of CLASP1, despite their very different inherent stabilities in the absence of CLASP1 (Fig. 2, G and H). Notably, in the presence of CLASP1 and GTP, the mean depolymerization rates were 9 ± 1 nm/s (SE, *N* = 30) for mixed-lattice microtubules, and 11 ± 2 nm/s (SE, *N* = 33) for GDP-lattice microtubules and were not statistically significantly different (*P* = 0.51). Similarly, the depolymerization rates in the presence of CLASP1 and GDP were the same on mixed-nucleotide lattices and GDP lattices (~ 10 nm/s; *P* = 0.91). Finally, both microtubule substrates were stable in the presence of CLASP1 and GMPCPP (~ 0.5 nm/s; *P* = 0.14). Therefore, our data show that CLASP1 dictates the stability of microtubule ends in a nucleotide-dependent manner and maintains the ends in a slowly depolymerizing pre-catastrophe state in the presence of GTP.

A minimal TOG2 domain construct is sufficient to induce stabilized microtubule depolymerization

All major isoforms of human CLASPs (CLASP1 α , CLASP2 α , and CLASP2 γ ; Fig. 3 A) suppress microtubule catastrophe (Lawrence et al., 2020; Lawrence et al., 2018; Yu et al., 2016; Aher et al., 2018; Lawrence and Zanic, 2019). Based on our hypothesis that stabilization of a pre-catastrophe intermediate state is the mechanism underlying both CLASP1's anti-catastrophe activity as well as its ability to promote depolymerization of stabilized microtubules, we wondered if other CLASP isoforms would also promote stabilized microtubule depolymerization. To address this, we incubated GMPCPP-stabilized microtubules with 200 nM of CLASP1, CLASP2 α , or CLASP2 γ and 1 mM GTP (Fig. 3 B). While CLASP1 displayed the strongest depolymerase activity, we found that all CLASP family members promoted depolymerization of stabilized microtubules in the presence of GTP (Fig. 3, B and C).

Previous work established that a minimal construct of CLASP2 α composed of a short linker region, the TOG2 domain and the serine-arginine-rich region (L-TOG2-S) recapitulates the anti-catastrophe and rescue activity of full-length human CLASP2 α on dynamically growing microtubules (Aher et al., 2018). Thus, we tested whether the L-TOG2-S construct also

possesses microtubule depolymerase activity. Indeed, we observed microtubule depolymerization when microtubules were incubated with 200 nM EGFP-tagged L-TOG2-S and 1 mM GTP (Fig. 3, B and C). The depolymerization rates of microtubules with all CLASP family members and the minimal L-TOG2-S domain construct were statistically significantly different from the control (*P* < 0.001, one-way ANOVA followed by a post hoc Tukey HSD). The finding that the minimal L-TOG2-S construct is capable of depolymerizing stable microtubules demonstrates that CLASP's depolymerase activity does not strictly require a string of multiple TOG domains. Furthermore, a previous report found that the isolated human TOG2 domain does not bind soluble tubulin (Aher et al., 2018), suggesting that both anti-catastrophe and depolymerase activity do not rely on direct interactions with soluble tubulin. Interestingly, the depolymerization rates with L-TOG2-S were significantly different from those with CLASP2 α , but not CLASP2 γ , suggesting that the TOG1 domain may contribute to CLASP's depolymerizing activity. Furthermore, the fact that L-TOG2-S is also the minimal unit required for CLASP's anti-catastrophe and rescue activities (Aher et al., 2018) supports the hypothesis that the molecular mechanisms underlying CLASP's ability to promote depolymerization are linked to its mechanism of microtubule dynamics regulation.

The binding of CLASP1 and TOG2 to microtubule ends is modulated by nucleotides

We next investigated the effects of the nucleotide in solution on the CLASP1's localization on stabilized microtubules. To this end, we incubated GMPCPP-stabilized microtubules with 1 nM Alexa 488-labeled-CLASP1 in the presence of different nucleotides. When no nucleotide was present in the solution, CLASP1 displayed clear microtubule end-binding preference (Fig. 4 A). The observed end-binding preference of CLASP1 is similar to previous observations of full-length CLASP2 γ , which preferentially associates with the plus-ends of stabilized microtubules in the absence of GTP (Lawrence et al., 2018). We also observed instances where CLASP1 localized to both microtubule ends (e.g., see Fig. 4, A and B, no nucleotide condition). Notably, CLASP1's enhanced end-localization was lost when GTP was present in the solution (Fig. 4, A and B). This is consistent with a recent study demonstrating that the localization of CLASP2 α on microtubule ends is lost with GTP (Luo et al., 2023). Furthermore, we observed preferential binding of CLASP1 to microtubule ends with the addition of GMPCPP, but not with the addition of GDP (Fig. 4, A and B). In other words, CLASP1 accumulated at the microtubule ends only in conditions that are incompatible with CLASP-mediated microtubule depolymerization (i.e., the no nucleotide and GMPCPP in solution conditions), but did not accumulate at the microtubule ends in conditions compatible with depolymerization (i.e., the GTP and GDP in solution conditions). These observations suggest that in the presence of GTP or GDP individual CLASP1 molecules dissociate from microtubule ends after nucleotide exchange has occurred.

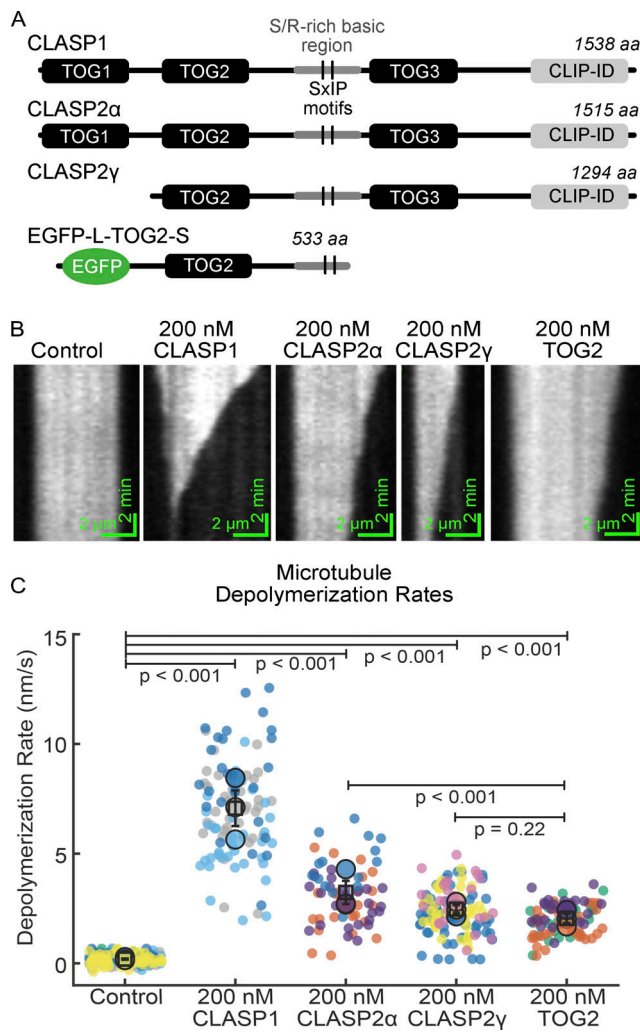


Figure 3. A minimal TOG2 domain construct is sufficient to induce stabilized microtubule depolymerization. (A) Domain structures of human CLASP family members and an EGFP-tagged TOG2 domain from CLASP2α. (B) Representative kymographs of GMPCPP-stabilized microtubules incubated with storage buffer, 200 nM CLASP1, 200 nM CLASP2α, 200 nM CLASP2γ, or 200 nM EGFP-L-TOG2-S in the presence of 1 mM GTP. (C) Quantification of microtubule depolymerization rates for the conditions in B. The mean rates of microtubule depolymerization are: 0.19 ± 0.03 nm/s (SE; $N = 221$ microtubules) for the buffer control, 7.1 ± 0.8 nm/s (SE; $N = 102$ microtubules) for CLASP1, 3.2 ± 0.5 nm/s (SE; $N = 70$ microtubules) for CLASP2α, 2.4 ± 0.2 nm/s (SE; $N = 100$ microtubules) for CLASP2γ, and 2.0 ± 0.2 nm/s (SE; $N = 86$ microtubules) for L-TOG2-S. All data were obtained across at least three different experimental days, and individual data points from different experiments are plotted in different shades. The means for each experimental repeat are plotted as larger points in the same color. The squares indicate the average of the experimental means, and the vertical bars are the standard errors of the means. Statistical significance was determined using a one-way ANOVA followed by Tukey's HSD test for multiple comparisons, and the corresponding P values are indicated on the graph.

To gain further insight into the depolymerase activity on a molecular level, we investigated whether GTP affects the duration of single-molecule L-TOG2-S binding events on microtubule ends. GMPCPP-stabilized microtubules were incubated with 200 pM EGFP-L-TOG2-S in the presence and absence of 1 mM GTP and imaged at 20 fps. We observed that L-TOG2-S also

exhibited microtubule end preference in the absence of GTP (Fig. 4 C). In the absence of GTP, the dwell times of L-TOG2-S on microtubule ends were long, with a mean dwell time of 3.8 ± 0.3 s (SE, $N = 405$). In contrast, in the presence of GTP, the dwell times of L-TOG2-S on microtubule ends were significantly shorter (0.53 ± 0.06 s; SE, $N = 708$, $P < 0.001$ compared to the no nucleotide condition, Mann-Whitney test; Fig. 4 D). Our measurements of microtubule depolymerization rates in the presence of L-TOG2-S and GTP correspond to the removal of one tubulin dimer every ~ 0.3 s on average (for an overall depolymerization rate of ~ 2 nm/s, Fig. 2 C), remarkably similar to the single-molecule dwell times in the presence of GTP. We thus speculate that microtubule depolymerization occurs through TOG2-mediated conformational change occurring at the microtubule end in a nucleotide-dependent manner.

CLASP1 promotes the depolymerization of microtubule plus and minus ends in the presence of GTP but is plus-end specific in the presence of GDP

Our investigation of CLASP1's localization revealed occasional binding to both microtubule ends (Fig. 4 A). Moreover, in our depolymerization assays, we noticed intriguing differences in the behavior of the two microtubule ends in the presence of CLASP1 with different nucleotides (Fig. 1 and Fig. S2). To determine the end-specific activity of CLASP1, we performed a titration of CLASP1 concentration from 0 to 500 nM in the presence of 1 mM GTP on polarity-marked GMPCPP-stabilized microtubules, allowing us to distinguish plus and minus ends (see Materials and methods; Fig. 5, A–C and Video 2). We found that the microtubule depolymerization rates increased with increasing CLASP1 concentrations at both plus and minus ends (Fig. 5, B and C). Fitting the CLASP1 titration data to the Michaelis-Menten equation revealed that the half-maximum depolymerization rate was achieved at 15 nM CLASP1 (95% CI: 10–20 nM) for plus ends, and 42 nM (95% CI: 5–79 nM) for minus ends (Fig. 5 C). Therefore, CLASP1 induces depolymerization at both microtubule plus and minus ends in the presence of GTP, but the plus ends are more susceptible to CLASP1-mediated depolymerization than the minus ends.

Due to the head-to-tail assembly of tubulin dimers in the microtubule lattice, microtubule minus ends do not possess an exposed nucleotide-binding site (Nogales et al., 1999). One explanation for the observation that CLASP1 promotes depolymerization of both microtubule ends in a nucleotide-dependent manner is that CLASP1 mediates nucleotide exchange at both microtubule ends, thus promoting subsequent end destabilization. Since the nucleotide-binding pocket is buried in the lattice at the minus end, CLASP1-mediated depolymerization of minus ends raises the possibility that CLASP1 can mediate nucleotide exchange all along the microtubule lattice.

To investigate the potential effects of CLASP1 on lattice nucleotide exchange, we performed computational modeling in which nucleotide exchange was permitted to occur either exclusively at microtubule ends or at both ends and lattice (Fig. S4). We assessed the depolymerization profiles of microtubules simulated to have mean depolymerization rates matching the experimentally observed rates. When nucleotide exchange was

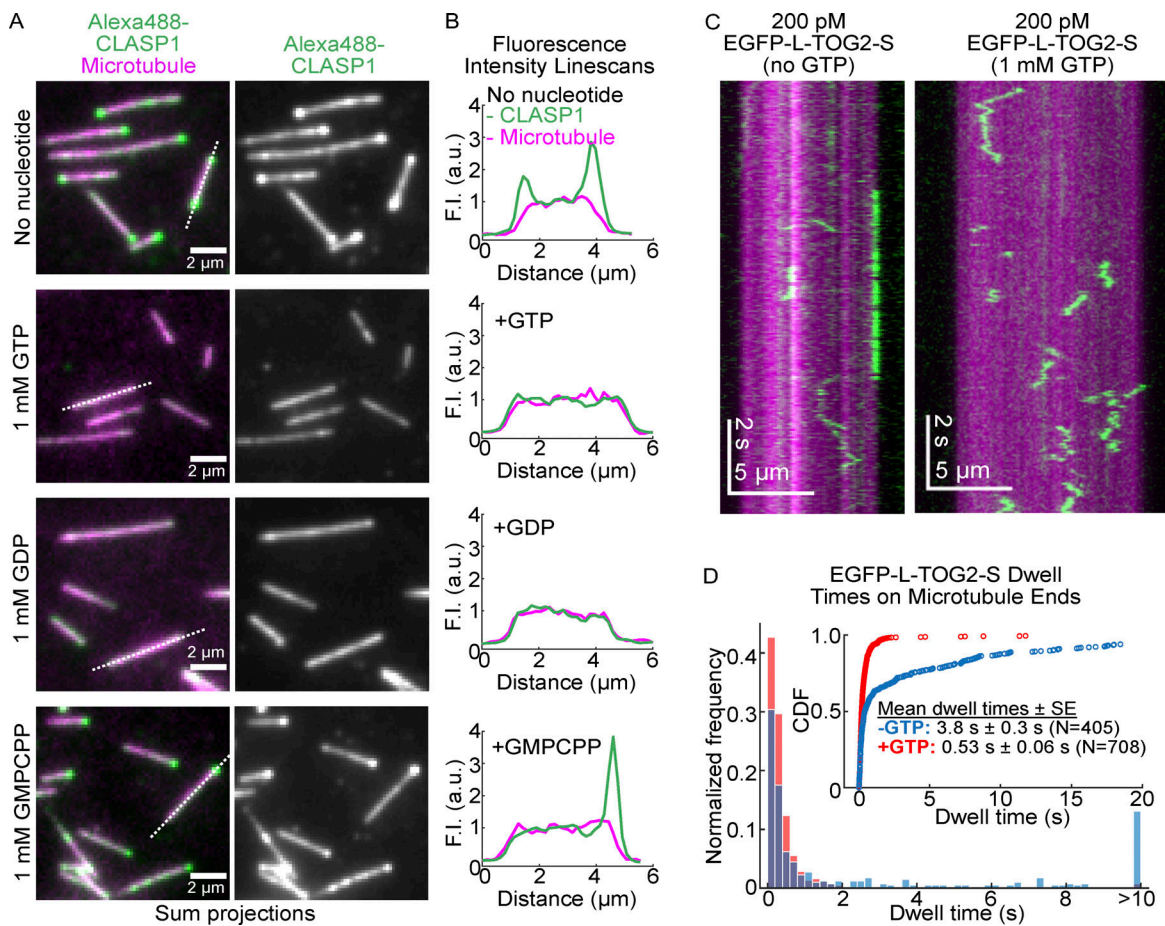


Figure 4. The binding of CLASP1 and TOG2 to microtubule ends is modulated by nucleotides. (A) Representative sum projection images of 1 nM Alexa488-CLASP1 on GMPCPP-stabilized microtubules in the absence or presence of the indicated nucleotide. Images are sum-projections of the 488-CLASP1 intensities from the first 5 s (100 frames) of 30-s videos imaged at 20 fps. The dotted lines indicate the positions of the corresponding linescans. **(B)** Fluorescence intensity linescans of the microtubules indicated by the dotted lines in A. **(C)** Representative kymographs of GMPCPP-stabilized microtubules incubated with 200 pM EGFP-L-TOG2-S with and without 1 mM GTP and imaged at 20 fps. **(D)** Quantification of the single-molecule EGFP-L-TOG2-S dwell times on GMPCPP-stabilized microtubules in the presence and absence of 1 mM GTP. The inset shows the cumulative distribution function of the data. *N* is the number of EGFP-L-TOG2-S binding events measured across three independent experimental repeats.

simulated to occur at both ends and lattice, the characteristics of the microtubule depolymerization were very different from those observed in experiments. Specifically, the simulated microtubules displayed highly nonlinear depolymerization profiles, with depolymerization rates accelerating over time due to the exposure of unstable lattice-exchanged dimers. In contrast, when nucleotide exchange was permitted only at microtubule ends, the depolymerization rates were constant over time, as observed in our experimental results. Therefore, our simulations argue against a mechanism whereby CLASP1 promotes minus-end depolymerization by facilitating nucleotide exchange throughout the microtubule lattice. Rather, we conclude that CLASP1 promotes the depolymerization of both plus and minus ends primarily through an end-specific mechanism.

Interestingly, we observed that, while CLASP1 depolymerized both of the microtubule ends in the presence of GTP, only one end appeared to depolymerize in the presence of GDP (Fig. S2). To investigate this further, we assessed the depolymerase activity of 200 nM CLASP1 on polarity-marked microtubules across a range of GTP and GDP concentrations (from 0 to 1 mM;

Fig. 5, D–F). As before, CLASP1-induced depolymerization of both microtubule plus and minus ends with GTP in solution, however, only plus ends depolymerized with GDP (Fig. 5 D). The rates of CLASP1-mediated microtubule depolymerization increased with increasing GTP concentrations at both plus and minus ends (Fig. 5 E). The half-maximum depolymerization rate was achieved at 0.12 mM GTP (95% CI: 0.06–0.18 mM) for plus ends, and 0.6 mM GTP (95% CI: 0.2–1.1 mM) for minus ends. Notably, CLASP1 enhanced the depolymerization of plus ends to a greater extent than minus ends: CLASP1 accelerated the depolymerization rate by 55-fold at the plus ends, and by 40-fold at the minus ends when comparing the 0 mM GTP condition to the saturating GTP concentration (V_{max}) for each end. In comparison, the depolymerization rate increased in a less sensitive manner with increasing GDP concentrations at microtubule plus ends, eventually reaching a similar rate to the GTP condition at the highest nucleotide concentration tested (1 mM; Fig. 5 F). Strikingly, we observed no depolymerization at minus ends with CLASP1 at any GDP concentration tested (slope not significantly different from zero; $P = 0.08$, *F* test for linear regression).

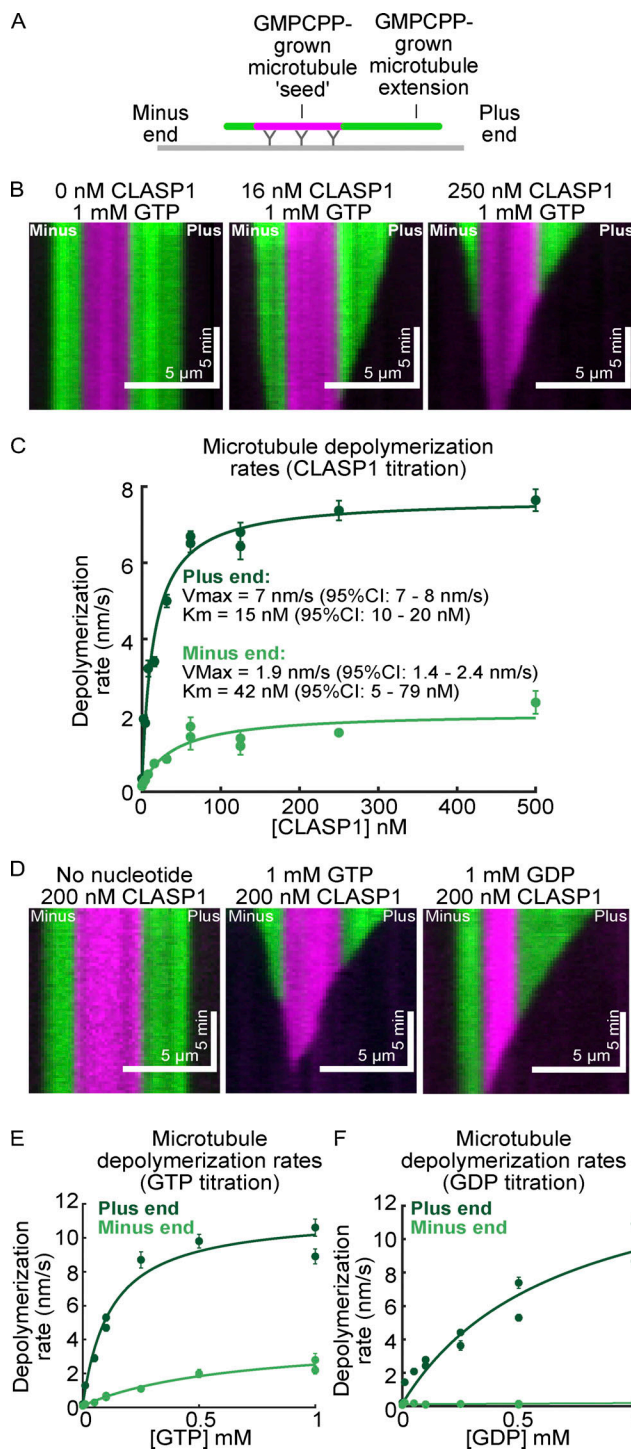


Figure 5. CLASP1 promotes the depolymerization of plus and minus ends in the presence of GTP but is plus-end specific in the presence of GDP. (A) Schematic of the polarity-marked microtubule assay used to distinguish plus and minus ends. (B) Representative kymographs of polarity-marked microtubules incubated with 0, 16, and 250 nM CLASP1. (C) Quantification of microtubule depolymerization rates as a function of CLASP1 concentration in the presence of 1 mM GTP. Data are means \pm SE; $N = 10$ microtubules analyzed per condition obtained from four experimental days. The solid lines represent the Michaelis-Menten fit to the data. (D) Representative kymographs of polarity-marked microtubules incubated with 200 nM CLASP1 in the no nucleotide, 1 mM GTP, and 1 mM GDP conditions. (E) Quantification of microtubule depolymerization rates as a function of GTP

Therefore, regardless of nucleotide, microtubule plus ends are more sensitive to CLASP1 than minus ends. Furthermore, the finding that CLASP1 induces depolymerization of minus ends with GTP, but not GDP, points to potentially distinct requirements for the removal of tubulin from the microtubule minus end. Overall, the distinct behaviors of the two microtubule ends are consistent with the previous report that the kinetics of the metastable intermediate state differ significantly between plus and minus ends (Tran et al., 1997).

Discussion

We discovered that CLASP specifically stabilizes a nucleotide-dependent intermediate state of the microtubule end as it transitions from growth to shrinkage. On stable microtubules, the ability of CLASP to promote the intermediate state manifests as slow but robust microtubule depolymerization. On dynamic microtubules, CLASP-mediated stabilization of the pre-catastrophe intermediate results in a microtubule end that is maintained in a slowly depolymerizing state even in the absence of soluble tubulin. Remarkably, we find that, in the presence of GTP, CLASP drives both stable and unstable microtubule ends into the same slowly depolymerizing state (in the 10 nm/s range, Figs. 1, 2, and 5), despite their vastly different inherent stabilities. These observations can be unified by a model in which CLASP promotes an intermediate state between microtubule growth and shrinkage (Fig. 6). We propose that the stabilization of microtubule ends in a pre-catastrophe intermediate state underlies the mechanism of CLASP's physiological role as an anti-catastrophe factor.

Our finding that CLASP promotes the depolymerization of stabilized microtubules in the presence of GTP but not in the absence of nucleotide in solution demonstrates that CLASP's activity is nucleotide dependent. Consistent with these results, a recent study reconstituting CLASP2-mediated kinetochore-microtubule interactions reported nucleotide sensitivity of the CLASP-microtubule attachments (Luo et al., 2023). Here, the authors used DNA origami to design clusters of CLASP2, which formed sustained load-bearing attachments to stabilized microtubule ends. The authors found that CLASP's attachment to microtubules was abrogated in the presence of GTP, which is expected to exchange spontaneously with nucleotide bound to the terminal tubulin subunits at stabilized microtubule ends (Luo et al., 2023; Mitchison, 1993). In agreement, CLASP's localization at stabilized microtubule ends is lost in the presence of

concentration in the presence of 200 nM CLASP1. Data are means \pm SE; $N = 10$ microtubules analyzed per condition obtained from three experimental days. The plus-end data are in dark green and the minus-end data are in light green. The solid lines represent the Michaelis-Menten fit to the data. See also Video 2. (F) Quantification of microtubule depolymerization rates as a function of GDP concentration in the presence of 200 nM CLASP1. Data are means \pm SE; $N = 10$ microtubules analyzed per condition obtained from four experimental days. The solid lines represent the Michaelis-Menten fit to the data for the plus end and a linear fit for the minus end. An F test for linear regression was performed to test the statistical significance of the minus-end data ($P = 0.08$).

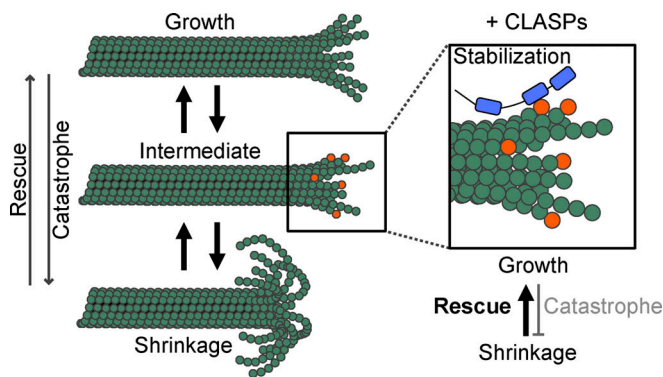


Figure 6. CLASPs stabilize an intermediate state between microtubule growth and shrinkage. Microtubules switch between growth and shrinkage through a metastable intermediate state, characterized by a unique nucleotide-dependent configuration of tubulin at the microtubule end (denoted in orange). CLASPs (purple) recognize and stabilize this intermediate state, thus suppressing catastrophe and promoting rescue.

GTP (Fig. 4; Luo et al., 2023; Lawrence et al., 2018), suggesting that CLASP does not recognize GTP-tubulin at microtubule ends. Indeed, CLASP does not localize efficiently to growing microtubule ends composed primarily of GTP-tubulin subunits in the absence of the microtubule-end targeting EB proteins (Lawrence et al., 2018; Aher et al., 2018). Furthermore, our results show that CLASP also promotes the depolymerization of stabilized microtubules in the presence of GTP γ S and GDP, but not GMPCPP, suggesting that CLASP's activity requires a post-GTP hydrolysis state. Interestingly, it has been proposed that the transient exposure of terminal GDP-tubulin dimers during growth serves as a precursor to catastrophe (Bowne-Anderson et al., 2013; Farmer and Zanic, 2023). However, CLASP does not localize to shrinking microtubule ends that display a flared protofilament morphology and are primarily composed of GDP-tubulin subunits (Aher et al., 2018; Lawrence et al., 2018). Thus, we speculate that CLASP acts on a unique and transient microtubule end configuration specific to the intermediate state.

CLASP's TOG2 domain has a unique architecture that permits binding to a distinct, highly curved conformation of tubulin (Lawrence et al., 2020; Leano et al., 2013; Maki et al., 2015; Leano and Slep, 2019). Previous reports demonstrated that minimal CLASP constructs containing the TOG2 domain prevent microtubule catastrophe (Aher et al., 2018; Majumdar et al., 2018). Furthermore, our results show that L-TOG2-S retains the ability of the full length protein to promote the depolymerization of stabilized microtubules (Fig. 3). We thus speculate that the unique tubulin conformation recognized by TOG2 is transiently probed by microtubule ends in the pre-catastrophe intermediate state. A previous study reported that the *Drosophila* homolog of CLASP recruits soluble tubulin to the microtubule lattice to promote rescue (Al-Bassam et al., 2010). Indeed, CLASPs can simultaneously interact with the microtubule lattice and soluble tubulin dimers (Fig. S3; Al-Bassam et al., 2010; Lawrence et al., 2018; Yu et al., 2016), and mutations in key tubulin-binding residues abolish CLASP's microtubule-stabilizing activity (Aher et al., 2018; Al-Bassam et al., 2010). However, the minimal L-TOG2-S construct prevents microtubule catastrophe despite

the fact that the isolated human TOG2 domain does not bind to soluble tubulin (Aher et al., 2018). Furthermore, we find that CLASP stabilizes dynamic microtubules against catastrophe upon soluble tubulin removal (Fig. 2). Interestingly, the polymerase mechanism of XMAP215 requires binding to soluble tubulin, and the presence of a stoichiometric amount of soluble tubulin switches XMAP215's activity from a depolymerase to a polymerase (Brouhard et al., 2008; Ayaz et al., 2012, 2014). In contrast, CLASP maintains its ability to promote the depolymerization of stabilized microtubules even in the presence of a 20-fold excess of soluble tubulin (Fig. S3). While the reversal of a microtubule end from a pre-catastrophe intermediate state back to growth can only happen in the presence of soluble tubulin, CLASP-mediated stabilization of the intermediate pre-catastrophe state occurs in the absence of soluble tubulin. Thus, our results suggest that CLASP's anti-catastrophe mechanism does not require direct interaction with tubulin dimers in solution.

CLASP's anti-catastrophe mechanism may involve facilitating nucleotide exchange in the terminal tubulin subunits. Indeed, exchanging GDP for GTP on the microtubule end was predicted to suppress microtubule catastrophe (Piedra et al., 2016). The transient exposure of GDP-tubulin at growing microtubule ends has recently been linked to an increase in microtubule growth fluctuations and slowed microtubule growth (Cleary et al., 2022). Notably, CLASP allows growing microtubule ends to withstand a greater degree of growth fluctuations and fosters the reversal of transient growth slowdowns into a microtubule growth state (Mahserejian et al., 2022; Lawrence et al., 2020). Importantly, CLASP does not suppress the rate of GTP hydrolysis, as evidenced by the size of the EB comets (Majumdar et al., 2018; Lawrence et al., 2018). Instead, CLASP may stabilize an otherwise transient pre-catastrophe state, allowing GDP-to-GTP nucleotide exchange on terminally exposed GDP-tubulin dimers and promoting a return to the growth phase. Interestingly, a previous study identified putative GTP-binding motifs in Orbit, the *Drosophila* homologue of CLASP (Inoue et al., 2000). However, these motifs are only partially conserved in human CLASP proteins (Luo et al., 2023). Furthermore, mutating the remaining conserved residues in human CLASP2 does not impact CLASP2's activity, suggesting that direct nucleotide binding by CLASP is not required for CLASP's mechanism (Luo et al., 2023).

While the nucleotide exchange at the terminal tubulin dimers microtubules occurs spontaneously on stabilized microtubules (Luo et al., 2023; Mitchison, 1993), our finding that the presence of GTP in solution does not lead to the depolymerization of GMPCPP-stabilized microtubules over the long timescales of our experiments (~30 min, Figs. 1 and 5) suggests that the terminal nucleotide exchange alone is not sufficient to destabilize the microtubule end. We thus speculate that, due to the unique structure of the TOG2 domain, CLASP's interaction with the microtubule end in the presence of GTP induces a distinct tubulin conformation leading to the observed slow depolymerization of stabilized microtubule ends. Alternatively, CLASP binding may facilitate nucleotide exchange in a buried penultimate tubulin subunit, inducing an allosteric effect at the

microtubule end (Kim and Rice, 2019; Ye et al., 2020; Geyer et al., 2015). The ability to facilitate nucleotide exchange in a buried tubulin subunit could help explain our finding that CLASP promotes the depolymerization of microtubule minus ends. Although nucleotide exchange can occur spontaneously at the minus ends, it does so less efficiently than at plus ends, likely due to the fact that the exchangeable site is buried within the lattice (Mitchison, 1993). Interestingly, a previous study found that TOG2-S preferentially binds ~10 tubulin layers behind the outmost end of the growing microtubule (Aher et al., 2018). Whether these binding sites correspond to tubulin subunits buried under a layer of terminally bound tubulin dimers or terminal tubulin dimers on lagging protofilaments at microtubule ends in a pre-catastrophe state is not known (Farmer et al., 2021; Aher et al., 2018; Doodhi et al., 2015). Thus, whether CLASP changes the tubulin conformation to facilitate nucleotide exchange or induces a post-exchange conformational change into a metastable intermediate remains to be determined and could be addressed by high-resolution structural studies.

The stabilization of a transient intermediate state of the microtubule end could also provide a mechanism for CLASP's rescue activity. Shrinking microtubule ends may stochastically and transiently probe the intermediate state, which is subsequently recognized and stabilized by CLASP, prompting a return to the growth phase. Rescue could also occur at sites of lattice defects, which may include missing tubulin subunits, changes in protofilament numbers or islands of GTP-tubulin. Indeed, it has recently been demonstrated that microtubule lattice damage repair sites act as sites of microtubule rescue when encountered by shrinking microtubule ends (Thery and Blanchoin, 2021; Aumeier et al., 2016). Damage sites are recognized by several MAPs, which may be involved in the process of lattice damage repair (Lawrence et al., 2021; van den Berg et al., 2023; Vemu et al., 2018; de Forges et al., 2016; Thery and Blanchoin, 2021). Interestingly, CLASP is implicated in microtubule lattice repair after damage, and just a few CLASP molecules at microtubule shrinking ends are sufficient to promote microtubule rescue (Aher et al., 2018; Aher et al., 2020). To what extent microtubule lattice damage and repair sites reflect the features of microtubule ends in the intermediate state is not known.

The recognition of distinct conformational states of the microtubule end facilitates combinatorial, multi-protein regulation of the microtubule dynamics. The EB-mediated targeting of CLASP to growing microtubule ends ensures that CLASP is readily available to catch its transient intermediate-state substrate as it appears at the end of microtubules transitioning to catastrophe. Unlike CLASP, XMAP215 autonomously tracks both growing and shrinking microtubule ends and simultaneously promotes microtubule growth and catastrophe (Farmer et al., 2021; Brouhard et al., 2008). CLASP's specific recognition of microtubule ends in the intermediate state ensures that CLASP and XMAP215 do not compete for the same tubulin substrate at microtubule ends, thus permitting both fast and persistent microtubule growth through the combined effects of both microtubule regulators (Arpag et al., 2020; Moriwaki and Goshima, 2016). Other MAPs, including EB1, MCAK, TPX2, and doublecortin, also recognize unique structural features of the microtubule

end related to tubulin nucleotide state, curvature and protofilament tapering (Reid et al., 2019; Bechstedt et al., 2014; Roostalu et al., 2015; Desai et al., 1999). Whether modulating the stability of the intermediate state is a general mechanism employed by MAPs to regulate microtubule dynamics is an exciting area for future research.

In conclusion, our results support a mechanism whereby CLASPs stabilize a nucleotide-dependent intermediate state of the microtubule end, which occurs as the microtubule transitions from growth to shrinkage. For dynamically growing microtubules, extending the period of time spent in the intermediate state allows the microtubule to re-enter the growth phase, thus avoiding catastrophe. We further propose that stabilizing the intermediate state underlies CLASP's mechanism of microtubule rescue. We, therefore, present a unifying mechanism underlying the two major activities of CLASP in suppressing catastrophe and promoting rescue. Overall, our discovery that CLASP1 stabilizes the intermediate state between microtubule growth and shrinkage in a nucleotide-dependent manner provides key mechanistic insights into an important family of microtubule regulatory proteins.

Materials and methods

DNA constructs

Human His-CLASP1 (NM_015282.2) in pFastBacHT vector was purchased from Genscript. The cDNA encoding full-length human CLASP2 α was purchased from Dharmacon (GenBank accession no. BC140778.1) and subcloned into a pFastBacHT vector (Invitrogen) containing an N-terminal 6xHis-tag. The His-CLASP2 γ construct was generated as previously described (Lawrence et al., 2018). The cDNA encoding His-EGFP-L-TOG2-S in a pRSETa vector was a gift from E. Grishchuk (University of Pennsylvania, Philadelphia, PA, USA; Luo et al., 2023). The plasmid containing chTOG cDNA was a gift from Stephen Royle (plasmid #69108; Addgene; <http://n2t.net/addgene:69108>; RRID: Addgene_69108). The chTOG cDNA was subcloned into a modified pFastBac vector containing an N-terminal 6xHis tag (a gift from G. Brouhard, McGill University, Montréal, QC, Canada). Cloning products were verified by DNA sequencing.

Protein preparation

Tubulin purification and fluorescent labeling

Bovine brain tubulin was purified using cycles of polymerization and depolymerization using the high-molarity PIPES method (Castoldi and Popov, 2003). Tubulin was labeled with tetramethylrhodamine (TAMRA) and Alexa Fluor 488 dyes (Thermo Fisher Scientific) according to the standard protocols and as previously described (Gell et al., 2010; Hyman et al., 1991). Fluorescently labeled tubulin was used at a ratio of between 5 and 25% of the total tubulin.

CLASP and chTOG protein purification

His-CLASP1 protein was expressed in baculovirus-infected Sf9 insect cells using the Bac-to-Bac system (Invitrogen). After the first amplification, baculovirus-infected insect cells (BIIC) stocks were used to infect Sf9 cells at a density of 1×10^6 viable cells/ml

at a ratio of 10^{-4} BIIC:total culture volume (Wasilko and Lee, 2006; Wasilko et al., 2009). Cells were harvested 5 d after infection. His-CLASP1 cell pellets were lysed by one freeze-thaw cycle and Dounce homogenizing in lysis buffer containing 50 mM HEPES (4-(2-hydroxyethyl)-1-piperazineethanesulfonic acid; pH 7.5), 150 mM NaCl, 2 mM $MgCl_2$, 5% (v/v) glycerol, 0.1% (v/v) Tween-20, 2 mM $MgCl_2$, 10 mM imidazole, 1 mM dithiothreitol (DTT) and supplemented with protease inhibitors. Genomic DNA was sheared by passing the lysate through an 18-gauge needle. The crude lysates were clarified by centrifugation for 20 min at 4°C and 35,000 rpm in a Beckman L90K Optima and 50.2 Ti rotor. Clarified lysates were applied to a HisTrapHP column (GE Lifesciences) according to the manufacturer's protocol. His-CLASP1 protein was eluted in 50 mM HEPES (pH 6.8), 150 mM NaCl, 5% (v/v) glycerol, 0.1% (v/v) Tween-20, 2 mM $MgCl_2$, 1 mM DTT, 50 mM L-glutamate, 50 mM L-arginine, and a linear gradient of 50–300 mM imidazole. His-CLASP1 was further purified and buffer exchanged into CLASP storage buffer (25 mM PIPES [piperazine-N,N'-bis(2-ethanesulfonic acid)], pH 6.8, 150 mM KCl, 5% (v/v) glycerol, 0.1% (v/v) Tween-20, 50 mM L-glutamate, 50 mM L-arginine, and 1 mM DTT) by size exclusion chromatography using a Superdex 200 Increase 10/300 GL column (Cytiva). Purified CLASP1 was labeled using Alexa Fluor 488 Microscale Protein Labeling Kit (cat. #A30006; Thermo Fisher Scientific) according to the manufacturer's instructions. His-CLASP2 α , His-CLASP2 γ proteins and His-EGFP-L-TOG2-S were expressed and purified as previously described (Lawrence et al., 2018; Rodgers et al., 2023).

His-chTOG protein was expressed in Sf9 insect cells and purified as described above for His-CLASP1 with the following modifications. Cell pellets were lysed in buffer containing 50 mM HEPES (pH 7.2), 400 mM KCl, 2 mM $MgCl_2$, 10% glycerol, 0.005% Brij35, 1 mM dithiothreitol (DTT) and supplemented with protease inhibitors. His-chTOG protein was eluted in 50 mM HEPES (pH 7.2), 400 mM KCl, 2 mM $MgCl_2$, 10% (v/v) glycerol, 0.005% (v/v) Brij35, 1 mM DTT, and a linear gradient of 60–400 mM imidazole. His-chTOG was further purified and exchanged into storage buffer (50 mM HEPES [pH 7.2], 400 mM KCl, 2 mM $MgCl_2$, 10% [v/v] glycerol, 0.005% [v/v] Brij35, 1 mM DTT) by size exclusion chromatography using a Superdex 200 Increase 10/300 GL column (Cytiva).

Protein purity was assessed by SDS-PAGE and/or mass spectrometry analysis. All proteins were snap-frozen in liquid nitrogen as single-use aliquots and stored at -80°C .

TIRF microscopy and microfluidic channel preparation

Imaging was performed using a Nikon Eclipse Ti microscope with a $100\times/1.49$ n.a. TIRF objective (Nikon), Andor iXon Ultra EM-CCD (electron multiplying charge-coupled device) camera (Andor); 488- and 561- solid-state lasers (Nikon Lu-NA); HS-625 high-speed emission filter wheel (Finger Lakes Instrumentation); and standard filter sets. For the data in Fig. S2, images were acquired with a Nikon high speed Ti-E microscope with epifluorescence, a $100\times/1.49$ TIRFApo objective and an Andor Neo 5.5 sCMOS camera (2560×2160 pixels, 1 pixel = 6.5×6.5 μm). In both cases, the microscopes were computer-controlled using Nikon Elements. A Tokai-Hit objective heater was used to

maintain the sample at 35°C for all experiments. Images were acquired with exposure times of 50–200 ms and at the frame rates specified in the methods.

Microscope chambers were constructed as previously described (Gell et al., 2010). Briefly, 22×22 and 18×18 mm silanized coverslips were separated by strips of Parafilm to create narrow channels for the exchange of solution. The channels were rinsed with BRB80 (80 mM PIPES adjusted to pH 6.8 with KOH, 1 mM $MgCl_2$, and 1 mM EGTA), incubated with 1:50 anti-TRITC antibody (#A-6397; Thermo Fisher Scientific) in BRB80 for 5 min, rinsed with BRB80, incubated with 1% Pluronic F127 in BRB80 for 30 min and rinsed again with BRB80.

GMPCPP-stabilized microtubule depolymerization assay

GMPCPP-stabilized microtubules (TAMRA-labeled) were prepared according to standard protocols (Gell et al., 2010). Microtubules were introduced into the imaging chamber and adhered to anti-TRITC antibody-coated coverslip surfaces. Reaction mixes containing concentrations of the proteins and nucleotides specified in the main text were introduced into the channels in imaging buffer. The imaging buffer consisted of BRB80 supplemented with 40 mM glucose, 40 $\mu\text{g}/\text{ml}$ glucose oxidase, 16 $\mu\text{g}/\text{ml}$ catalase, 0.5 mg/ml casein, 50 mM KCl, 10 mM DTT, and 1 mM $MgCl_2$. Microtubules were imaged for 15 min at a frame rate of 0.04 fps. Microtubule lengths were tracked over time with FIESTA (Ruhnnow et al., 2011) and used to calculate mean depolymerization rates for the first 5 min of depolymerization. For each individual microtubule, the filament length in every frame for the first 5 min of the video (0.04 fps) was plotted against time in MATLAB, and the depolymerization rates were determined from the slope of the linear regression line fitted to the data. Outliers were identified as $\pm 3 \times \text{SD}$ away from the mean and discarded. Data were plotted as “SuperPlots” in which individual data points and the corresponding means are color-coded by experimental repeat to represent the experimental variability (Lord et al., 2020).

Polarity-marked microtubule depolymerization assay

Polarity-marked microtubules were generated by polymerizing A488-labeled GMPCPP-tubulin extensions from TAMRA-labeled microtubule seeds with 3.5–5 μM A488-tubulin and 1 mM GMPCPP for 10 min in microfluidic channels. Since microtubules grown with GMPCPP do not undergo catastrophe and microtubule plus ends grow faster than minus ends, the two ends were distinguished by their lengths, with the longer extension designated as the plus end and the shorter extension as the minus end. Reaction mixes containing CLASP1 and nucleotides as indicated in the main text were introduced into the channels in imaging buffer, and microtubule depolymerization was imaged for 20 min at a frame rate of 0.04 fps. Microtubule depolymerization rates were determined independently for each end of the A448-GMPCPP-stabilized extensions on kymographs over the first 5 min of the experiment. Outliers were identified as $\pm 3 \times \text{SD}$ away from the mean and discarded. The depolymerization rates of plus and minus ends for the titrations of CLASP1, GTP, and GDP (plus-end only) were fit to the Michaelis-Menten equation:

$$v = \frac{v_{max}[S]}{K_d^h + [S]},$$

where v_{max} is the maximum depolymerization rate, K_m is the concentration at which half-maximum rate is achieved.

Tubulin dilution experiments

Microtubules with mixed-nucleotide and GDP lattices were polymerized in the microfluidic channels from GMPCPP-stabilized microtubule seeds. Mixed lattice extensions were grown with 7 μ M A488-tubulin and a nucleotide mixture containing 0.2 mM GTP and 0.8 mM GMPCPP for 20 min, resulting in microtubule lattices with an estimated nucleotide content of ~50% GTP and 50% GMPCPP (Tropini et al., 2012). GDP microtubules were grown with 12 μ M A488-tubulin and 1 mM GTP for 10 min. Buffer exchange was performed using filter paper to dilute soluble tubulin and introduce reaction mixtures containing nucleotides with or without 23 nM CLASP1 while imaging. Post-dilution, mixed-lattice microtubules were imaged for 15 min at a frame rate of 0.2 fps, and GDP-lattice microtubules were imaged at a frame rate of 1 fps for 5 min. Microtubule plus-end depolymerization rates were determined from kymographs for the first 5 min after dilution. Outliers were identified as $\pm 3 \times$ SD away from the mean and discarded. Data were plotted as “SuperPlots” as described above.

Single-molecule dwell time analysis

GMPCPP-stabilized microtubules were incubated for 2 min with 200 pM EGFP-L-TOG2-S or 1 nM A488-labelled CLASP1 to allow the reaction to equilibrate in the imaging chambers prior to imaging. For, EGFP-L-TOG2-S, images were acquired at 20 fps for 30 s using the maximum 488 nm laser power and 50 ms exposure. For 488-CLASP1, images were acquired at 2 fps for 5 min. An image of the microtubule seed was taken before and after the timelapse. The durations of the binding events on microtubule ends were measured from kymographs generated in Fiji (Schindelin et al., 2012) by manually marking the beginning and end of each event. Dwell times were plotted as histograms with 0.2 s (4-frame) bins and cumulative distribution frequency (CDF) plots in MATLAB.

Computational simulations

Microtubule destabilization due to nucleotide exchange was modeled at tubulin dimers incorporated in a microtubule. To implement the exchange kinetics at tubulin dimer level, we first project the hollow cylindrical manifold of a microtubule onto a two-dimensional lattice where each lattice node represents a site for the tubulin dimer (Fig. S4). For simplicity, we considered that all the protofilaments in a microtubule are of same length as the microtubule itself. The nucleotide exchange at a site was considered as a “change of state” of a tubulin dimer (as illustrated in Fig. S4, where, “green” sites turn into “blue” upon nucleotide exchange). The effective exchange rate at plus/minus ends was considered to be $K_{plus/minus} = k_{exchange}^{0-plus/minus} + k_{exchange}^{plus/minus} [M]$ where $[M]$ is the effective CLASP concentration, and $k_{exchange}^{0-plus/minus}$ corresponds to the rate of spontaneous depolymerization of GMPCPP microtubules in the absence of CLASP. Further, the probability of

exchange $p_{exchange}^{plus/minus}$ is defined as $(1 - \exp(-K_{plus/minus}\Delta t))$, where Δt denotes the time step chosen for the simulation.

In each iteration of the simulation, we scanned the columns at the microtubule ends and randomly visited all N_{pf} number of sites along the rows. Upon visiting a randomly picked microtubule end site, we drew a random number p between 0 and 1 from uniform distribution. If p is less than $p_{exchange}^{plus}$ at the plus end (or $p_{exchange}^{minus}$ at the minus end), we considered that the nucleotide exchange had occurred at the site under consideration. Through this iterative exchange process, if the number of exchanged sites at an exposed end column exceeds a pre-determined threshold value ($N_{threshold}$), that end column falls off. For our simulations, if not mentioned otherwise, $N_{threshold}$ was chosen to be 6 (Atherton et al., 2018). In the model, removal of a terminally exposed end column marks the depolymerization of a linear array of tubulin dimers at microtubule end, which shortens the microtubule length by 8 nm—the length of a single tubulin dimer (Fig. S4).

Next, we introduced the nucleotide exchange at tubulin dimers integrated within the microtubule lattice, in addition to microtubule ends. The rationale underlying this consideration is as follows. At plus ends, CLASP may facilitate nucleotide exchange from GMPCPP to GTP which acts as a precursor for terminal tubulin removal and depolymerization. However, at minus ends, the exchangeable nucleotide in the β -tubulin subunit is “buried” inside the lattice. Therefore, we reasoned that if the exchange can happen at the minus ends, it should also happen within the microtubule lattice. For this reason, we set the exchange rate within the lattice to be equal to the minus end exchange rate. The probability of lattice exchange $p_{exchange}^{lattice}$ is defined as $p_{exchange}^{lattice} = (1 - \exp(-K_{lattice}\Delta t))$, where $K_{lattice}$ is $k_{lattice}^{lattice} [M]$, and $k_{lattice}^{lattice}$ denotes the rate of lattice exchange per unit time per unit concentration. For simplicity, in simulations where lattice exchange was switched “on,” we set $k_{exchange}^{0-plus/minus}$ (the CLASP concentration-independent end exchange rate) to zero, as its effect was small compared to concentration-dependent exchange rates at microtubule ends. In the presence of lattice nucleotide exchange during each time step, if a terminally exposed column of dimers falls off, the adjacent column (the newly exposed one) also falls off iteratively if the number of exchanged sites at that column exceeds $N_{threshold}$.

The model parameters are listed in Table S2. The code for the agent-based nucleotide exchange simulations was written in MATLAB (The MathWorks) and is available at <https://github.com/ZanicLab/>. A single simulation run of microtubule depolymerization takes minutes of real-time in Apple M1 CPU, RAM 16 GB.

Statistical methods

Unless otherwise specified, statistical significance was analyzed using the unpaired Welch’s two-tailed unequal variances t tests on the means of the independent experimental replicates when comparing only two conditions; or by one-way ANOVA followed by Tukey’s HSD test for multiple comparisons when comparing multiple conditions, as indicated in the figure legends. Data distribution was assumed to be normal, but this was not formally tested. For the single molecule dwell time analysis in

Fig. 4, a non-parametric Mann-Whitney U test was performed and normality was not assumed. For the minus-end GDP titration data in Fig. 5, an *F* test for linear regression was performed to test if the slope was significantly non-zero. Additional details can be found in the figure legends. The statistical analyses were performed using GraphPad Prism and Statistics Kingdom (Statistics Kingdom, 2017).

Online supplemental material

Fig. S1 shows the purified proteins used in this manuscript. Fig. S2 shows the effects of different nucleotides and nucleotide analogs on CLASP's activity on stable microtubules. Fig. S3 shows the effects of soluble tubulin on CLASP's activity. Fig. S4 shows simulations of stable microtubule depolymerization. Video 1 shows the effects of CLASP1 on stable microtubules with and without GTP. Video 2 shows the effects of CLASP1 on microtubule plus and minus ends in the presence of GTP versus GTP alone. Table S1 lists the depolymerization rates of different microtubule substrates in the presence and absence of CLASP1, related to Fig. 2 C. Table S2 lists the model parameters used in simulations, related to Fig. S4. Data S1 contains the data underlying Figs. 1–5 and Figs. S2 and S3.

Data availability

The data are available in the published article and its online supplemental material. The MATLAB scripts for the agent-based nucleotide exchange simulations are available at <https://github.com/ZanicLab/>.

Acknowledgments

We thank S. Hall for help with protein purification, A. Maiorov and E. Grishchuk (University of Pennsylvania) for the kind gift of the EGFP-L-TOG2-S expression construct, and G. Brouhard (McGill University) for the modified pFastBac expression vector.

We also thank H. McDonald and the Vanderbilt Mass Spectrometry Research Center (MSRC) Cores for the mass spectrometry analysis, which was supported in part by Vanderbilt Ingram Cancer Center Resource Share Scholarship 2020-2909607. We thank members of the Zanic lab, A. Olivares, E. Grishchuk, and the Vanderbilt Microtubules and Motors Club for discussions and feedback. E.J. Lawrence acknowledges the support of the National Institutes of Health IBSTO training grant T32CA119925. M. Zanic acknowledges support from the National Institutes of Health grant R35GM119552.

Author contributions: E.J. Lawrence: conceptualization, methodology, investigation, formal analysis, validation, visualization, writing (original draft), writing (review and editing). S. Chatterjee: formal analysis, investigation, validation, software. M. Zanic: conceptualization, methodology, supervision, project administration, visualization, writing (original draft), writing (review and editing).

Disclosures: The authors declare no competing interests exist.

Submitted: 6 July 2021

Revised: 3 December 2022

Accepted: 18 April 2023

References

- Aher, A., M. Kolk, A. Sharma, A. Rai, N. Olieric, R. Rodriguez-Garcia, E.A. Katrukha, T. Weinert, V. Olieric, L.C. Kapitein, et al. 2018. CLASP suppresses microtubule catastrophes through a single TOG domain. *Dev. Cell.* 46:40–58.e8. <https://doi.org/10.1016/j.devcel.2018.05.032>
- Aher, A., D. Rai, L. Schaedel, J. Gaillard, K. John, Q. Liu, M. Altelaar, L. Blanchoin, M. Théry, and A. Akhmanova. 2020. CLASP mediates microtubule repair by Restricting lattice damage and regulating tubulin incorporation. *Curr. Biol.* 30:2175–2183.e6. <https://doi.org/10.1016/j.cub.2020.03.070>
- Akhmanova, A., C.C. Hoogenraad, K. Drabek, T. Stepanova, B. Dortland, T. Verkerk, W. Vermeulen, B.M. Burgering, C.I. De Zeeuw, F. Grosveld, and N. Galjart. 2001. Clasps are CLIP-115 and -170 associating proteins involved in the regional regulation of microtubule dynamics in motile fibroblasts. *Cell.* 104:923–935. [https://doi.org/10.1016/S0092-8674\(01\)00288-4](https://doi.org/10.1016/S0092-8674(01)00288-4)
- Al-Bassam, J., and F. Chang. 2011. Regulation of microtubule dynamics by TOG-domain proteins XMAP215/Dis1 and CLASP. *Trends Cell Biol.* 21: 604–614. <https://doi.org/10.1016/j.tcb.2011.06.007>
- Al-Bassam, J., H. Kim, G. Brouhard, A. van Oijen, S.C. Harrison, and F. Chang. 2010. CLASP promotes microtubule rescue by recruiting tubulin dimers to the microtubule. *Dev. Cell.* 19:245–258. <https://doi.org/10.1016/j.devcel.2010.07.016>
- Arpač, G., E.J. Lawrence, V.J. Farmer, S.L. Hall, and M. Zanic. 2020. Collective effects of XMAP215, EB1, CLASP2, and MCAK lead to robust microtubule treadmilling. *Proc. Natl. Acad. Sci. USA.* 117:12847–12855. <https://doi.org/10.1073/pnas.2003191117>
- Atherton, J., M. Stouffer, F. Francis, and C.A. Moores. 2018. Microtubule architecture in vitro and in cells revealed by cryo-electron tomography. *Acta Crystallogr. D Struct. Biol.* 74:572–584. <https://doi.org/10.1107/S2059798318001948>
- Aumeier, C., L. Schaedel, J. Gaillard, K. John, L. Blanchoin, and M. Théry. 2016. Self-repair promotes microtubule rescue. *Nat. Cell Biol.* 18: 1054–1064. <https://doi.org/10.1038/ncb3406>
- Ayaz, P., S. Munyoki, E.A. Geyer, F. Piedra, E.S. Vu, R. Bromberg, Z. Otwinowski, N.V. Grishin, C.A. Brautigam, and L.M. Rice. 2014. A tethered delivery mechanism explains the catalytic action of a microtubule polymerase. *Elife.* 3:e03069. <https://doi.org/10.7554/eLife.03069>
- Ayaz, P., X. Ye, P. Huddleston, C.A. Brautigam, and L.M. Rice. 2012. A TOG: $\alpha\beta$ -tubulin complex structure reveals conformation-based mechanisms for a microtubule polymerase. *Science.* 337(6096):857–860. <https://doi.org/10.1126/science.1221698>
- Bechstedt, S., K. Lu, and G.J. Brouhard. 2014. Doublecortin recognizes the longitudinal curvature of the microtubule end and lattice. *Curr. Biol.* 24: 2366–2375. <https://doi.org/10.1016/j.cub.2014.08.039>
- Bowne-Anderson, H., M. Zanic, M. Kauer, and J. Howard. 2013. Microtubule dynamic instability: A new model with coupled GTP hydrolysis and multistep catastrophe. *Bioessays.* 35:452–461. <https://doi.org/10.1002/bies.201200131>
- Brouhard, G.J., and L.M. Rice. 2014. The contribution of $\alpha\beta$ -tubulin curvature to microtubule dynamics. *J. Cell Biol.* 207:323–334. <https://doi.org/10.1083/jcb.201407095>
- Brouhard, G.J., J.H. Stear, T.L. Noetzel, J. Al-Bassam, K. Kinoshita, S.C. Harrison, J. Howard, and A.A. Hyman. 2008. XMAP215 is a processive microtubule polymerase. *Cell.* 132:79–88. <https://doi.org/10.1016/j.cell.2007.11.043>
- Castoldi, M., and A.V. Popov. 2003. Purification of brain tubulin through two cycles of polymerization-depolymerization in a high-molarity buffer. *Protein Expr. Purif.* 32:83–88. [https://doi.org/10.1016/S1046-5928\(03\)00218-3](https://doi.org/10.1016/S1046-5928(03)00218-3)
- Cleary, J.M., T. Kim, A.S.I. Cook, L.A. McCormick, W.O. Hancock, and L.M. Rice. 2022. Measurements and simulations of microtubule growth imply strong longitudinal interactions and reveal a role for GDP on the elongating end. *Elife.* 11:e75931. <https://doi.org/10.7554/eLife.75931>
- de Forges, H., A. Pilon, I. Cantaloube, A. Pallandre, A.M. Haghiri-Gosnet, F. Perez, and C. Poüs. 2016. Localized mechanical stress promotes microtubule rescue. *Curr. Biol.* 26:3399–3406. <https://doi.org/10.1016/j.cub.2016.10.048>
- Desai, A., S. Verma, T.J. Mitchison, and C.E. Walczak. 1999. Kin I kinesins are microtubule-destabilizing enzymes. *Cell.* 96:69–78. [https://doi.org/10.1016/S0092-8674\(00\)80960-5](https://doi.org/10.1016/S0092-8674(00)80960-5)
- Doodhi, H., A.E. Prota, R. Rodríguez-García, H. Xiao, D.W. Custer, K. Bargsten, E.A. Katrukha, M. Hilbert, S. Hua, K. Jiang, et al. 2015. Termination of protofilament elongation by eribulin induces lattice defects that promote microtubule catastrophes. *Curr. Biol.* 26:1713–1721. <https://doi.org/10.1016/j.cub.2016.04.053>

- Duellberg, C., N.I. Cade, D. Holmes, and T. Surrey. 2016. The size of the EB cap determines instantaneous microtubule stability. *Elife*. 5:1–23. <https://doi.org/10.7554/eLife.13470>
- Farmer, V., G. Arpag, S.L. Hall, and M. Zanic. 2021. XMAP215 promotes microtubule catastrophe by disrupting the growing microtubule end. *J. Cell Biol.* 220:e202012144. <https://doi.org/10.1083/jcb.202012144>
- Farmer, V.J., and M. Zanic. 2021. TOG-domain proteins. *Curr. Biol.* 31: R499–R501. <https://doi.org/10.1016/j.cub.2021.01.039>
- Farmer, V.J., and M. Zanic. 2023. Beyond the GTP-cap: Elucidating the molecular mechanisms of microtubule catastrophe. *Bioessays*. 45:e2200081. <https://doi.org/10.1002/bies.202200081>
- Funk, C., V. Schmeiser, J. Ortiz, and J. Lechner. 2014. A TOGL domain specifically targets yeast CLASP to kinetochores to stabilize kinetochore microtubules. *J. Cell Biol.* 205:555–571. <https://doi.org/10.1083/jcb.201310018>
- Gell, C., V. Bormuth, G.J. Brouhard, D.N. Cohen, S. Diez, C.T. Friel, J. Helenius, B. Nitzsche, H. Petzold, J. Ribbe, et al. 2010. Microtubule dynamics reconstituted in vitro and imaged by single-molecule fluorescence microscopy. *Methods Cell Biol.* 95:221–245. [https://doi.org/10.1016/S0091-679X\(10\)95013-9](https://doi.org/10.1016/S0091-679X(10)95013-9)
- Geyer, E.A., A. Burns, B.A. Lalonde, X. Ye, F.A. Piedra, T.C. Huffaker, and L.M. Rice. 2015. A mutation uncouples the tubulin conformational and GTPase cycles, revealing allosteric control of microtubule dynamics. *Elife*. 4:e10113. <https://doi.org/10.7554/eLife.10113>
- Gudimchuk, N.B., and J.R. McIntosh. 2021. Regulation of microtubule dynamics, mechanics and function through the growing tip. *Nat. Rev. Mol. Cell Biol.* 22:777–795. <https://doi.org/10.1038/s41580-021-00399-x>
- Hyman, A., D. Drechsel, D. Kellogg, S. Salsler, K. Sawin, P. Steffen, L. Wordeman, and T. Mitchison. 1991. Preparation of modified tubulins. *Methods Enzymol.* 196:478–485. [https://doi.org/10.1016/0076-6879\(91\)96041-0](https://doi.org/10.1016/0076-6879(91)96041-0)
- Inoue, Y.H., M. do Carmo Avides, M. Shiraki, P. Deak, M. Yamaguchi, Y. Nishimoto, A. Matsukage, and D.M. Glover. 2000. Orbit, a novel microtubule-associated protein essential for mitosis in *Drosophila melanogaster*. *J. Cell Biol.* 149:153–166. <https://doi.org/10.1083/jcb.149.1.153>
- Jánosi, I.M., D. Chrétien, and H. Flyvbjerg. 2002. Structural microtubule cap: Stability, catastrophe, rescue, and third state. *Biophys. J.* 83:1317–1330. [https://doi.org/10.1016/S0006-3495\(02\)73902-7](https://doi.org/10.1016/S0006-3495(02)73902-7)
- Kim, T., and L.M. Rice. 2019. Long-range, through-lattice coupling improves predictions of microtubule catastrophe. *Mol. Biol. Cell.* 30:1451–1462. <https://doi.org/10.1091/mbc.E18-10-0641>
- Lawrence, E.J., G. Arpag, C. Arnaiz, and M. Zanic. 2021. SSNA1 stabilizes dynamic microtubules and detects microtubule damage. *Elife*. 10:e67282. <https://doi.org/10.7554/eLife.67282>
- Lawrence, E.J., G. Arpag, S.R. Norris, and M. Zanic. 2018. Human CLASP2 specifically regulates microtubule catastrophe and rescue. *Mol. Biol. Cell.* 29:1168–1177. <https://doi.org/10.1091/mbc.E18-01-0016>
- Lawrence, E.J., and M. Zanic. 2019. Rescuing microtubules from the brink of catastrophe: CLASPs lead the way. *Curr. Opin. Cell Biol.* 56:94–101. <https://doi.org/10.1016/j.ceb.2018.10.011>
- Lawrence, E.J., M. Zanic, and L.M. Rice. 2020. CLASPs at a glance. *J. Cell Sci.* 133:jcs243097. <https://doi.org/10.1242/jcs.243097>
- Leano, J.B., S.L. Rogers, and K.C. Slep. 2013. A cryptic TOG domain with a distinct architecture underlies CLASP-dependent bipolar spindle formation. *Structure*. 21:939–950. <https://doi.org/10.1016/j.str.2013.04.018>
- Leano, J.B., and K.C. Slep. 2019. Structures of TOG1 and TOG2 from the human microtubule dynamics regulator CLASP1. *PLoS One*. 14:e0219823. <https://doi.org/10.1371/journal.pone.0219823>
- Li, W., T. Moriwaki, T. Tani, T. Watanabe, K. Kaibuchi, and G. Goshima. 2012. Reconstitution of dynamic microtubules with *Drosophila* XMAP215, EB1, and Sentin. *J. Cell Biol.* 199:849–862. <https://doi.org/10.1083/jcb.201206101>
- Lord, S.J., K.B. Velle, R.D. Mullins, and L.K. Fritz-Laylin. 2020. SuperPlots: Communicating reproducibility and variability in cell biology. *J. Cell Biol.* 219:e202001064. <https://doi.org/10.1083/jcb.202001064>
- Luo, W., V. Demidov, Q. Shen, H. Girão, M. Chakraborty, A. Maiorov, F.I. Ataullakhanov, C. Lin, H. Maiato, and E.L. Grishchuk. 2023. CLASP2 recognizes tubulins exposed at the microtubule plus-end in a nucleotide state-sensitive manner. *Sci. Adv.* 9:eabq5404. <https://doi.org/10.1126/sciadv.abq5404>
- Mahserejian, S.M., J.P. Scripture, A.J. Mauro, E.J. Lawrence, E.M. Jonasson, K.S. Murray, J. Li, M. Gardner, M. Alber, M. Zanic, and H.V. Goodson. 2022. Quantification of microtubule stutters: Dynamic instability behaviors that are strongly associated with catastrophe. *Mol. Biol. Cell.* 33: ar22. <https://doi.org/10.1091/mbc.E20-06-0348>
- Majumdar, S., T. Kim, Z. Chen, S. Munyoki, S.C. Tso, C.A. Brautigam, and L.M. Rice. 2018. An isolated CLASP TOG domain suppresses microtubule catastrophe and promotes rescue. *Mol. Biol. Cell.* 29:1359–1375. <https://doi.org/10.1091/mbc.E17-12-0748>
- Maki, T., A.D. Grimaldi, S. Fuchigami, I. Kaverina, and I. Hayashi. 2015. CLASP2 has two distinct TOG domains that contribute differently to microtubule dynamics. *J. Mol. Biol.* 427:2379–2395. <https://doi.org/10.1016/j.jmb.2015.05.012>
- Mangeol, P., B. Prevo, and E.J.G. Peterman. 2016. KymographClear and KymographDirect: two tools for the automated quantitative analysis of molecular and cellular dynamics using kymographs. *Mol Biol Cell.* 27(12):1948–1957. <https://doi.org/10.1091/mbc.E15-06-0404>
- Maurer, S.P., N.I. Cade, G. Bohner, N. Gustafsson, E. Boutant, and T. Surrey. 2014. EB1 accelerates two conformational transitions important for microtubule maturation and dynamics. *Curr. Biol.* 24:372–384. <https://doi.org/10.1016/j.cub.2013.12.042>
- Mitchison, T., and M. Kirschner. 1984. Dynamic instability of microtubule growth. *Nature*. 312:237–242. <https://doi.org/10.1038/312237a0>
- Mitchison, T.J. 1993. Localization of an exchangeable GTP binding site at the plus end of microtubules. *Science*. 261:1044–1047. <https://doi.org/10.1126/science.8102497>
- Moriwaki, T., and G. Goshima. 2016. Five factors can reconstitute all three phases of microtubule polymerization dynamics. *J. Cell Biol.* 215: 357–368. <https://doi.org/10.1083/jcb.201604118>
- Nogales, E., M. Whittaker, R.A. Milligan, and K.H. Downing. 1999. High-resolution model of the microtubule. *Cell*. 96:79–88. [https://doi.org/10.1016/S0092-8674\(00\)80961-7](https://doi.org/10.1016/S0092-8674(00)80961-7)
- Piedra, F.A., T. Kim, E.S. Garza, E.A. Geyer, A. Burns, X. Ye, and L.M. Rice. 2016. GDP-to-GTP exchange on the microtubule end can contribute to the frequency of catastrophe. *Mol. Biol. Cell.* 27:3515–3525. <https://doi.org/10.1091/mbc.e16-03-0199>
- Reid, T.A., C. Coombes, S. Mukherjee, R.R. Goldblum, K. White, S. Parmar, M. McClellan, M. Zanic, N. Courtemanche, and M.K. Gardner. 2019. Structural state recognition facilitates tip tracking of EB1 at growing microtubule ends. *Elife*. 8:e48117. <https://doi.org/10.7554/eLife.48117>
- Rodgers, N.C., E.J. Lawrence, A.V. Sawant, N. Efimova, G. Gonzalez-Vasquez, T.T. Hickman, I. Kaverina, and M. Zanic. 2023. CLASP2 facilitates dynamic actin filament organization along the microtubule lattice. *Mol. Biol. Cell.* 34:br3. <https://doi.org/10.1091/mbc.E22-05-0149>
- Roostalu, J., N.I. Cade, and T. Surrey. 2015. Complementary activities of TPX2 and chTOG constitute an efficient importin-regulated microtubule nucleation module. *Nat. Cell Biol.* 17:1422–1434. <https://doi.org/10.1038/ncb3241>
- Ruhnow, F., D. Zwicker, and S. Diez. 2011. Tracking single particles and elongated filaments with nanometer precision. *Biophys. J.* 100: 2820–2828. <https://doi.org/10.1016/j.bpj.2011.04.023>
- Schindelin, J., I. Arganda-Carreras, E. Frise, V. Kaynig, M. Longair, T. Pietzsch, S. Preibisch, C. Rueden, S. Saalfeld, B. Schmid, et al. 2012. Fiji: An open-source platform for biological-image analysis. *Nat. Methods*. 9: 676–682. <https://doi.org/10.1038/nmeth.2019>
- Slep, K.C. 2009. The role of TOG domains in microtubule plus end dynamics. *Biochem. Soc. Trans.* 37:1002–1006. <https://doi.org/10.1042/BST0371002>
- Sousa, A., R. Reis, P. Sampaio, and C.E. Sunkel. 2007. The *Drosophila* CLASP homologue, Mast/Orbit regulates the dynamic behaviour of interphase microtubules by promoting the pause state. *Cell Motil. Cytoskeleton*. 64: 605–620. <https://doi.org/10.1002/cm.20208>
- Statistics Kingdom. 2017. *Statistics Kingdom*. <http://www.statskingdom.com> [Accessed 9 April 2023]
- Strothman, C., V. Farmer, G. Arpag, N. Rodgers, M. Podolski, S. Norris, R. Ohi, and M. Zanic. 2019. Microtubule minus end stability is dictated by the tubulin off-rate. *J. Cell Biol.* 218:2841–2853. <https://doi.org/10.1083/jcb.201905019>
- Théry, M., and L. Blanchoin. 2021. Microtubule self-repair. *Curr. Opin. Cell Biol.* 68:144–154. <https://doi.org/10.1016/j.ceb.2020.10.012>
- Tran, P.T., R.A. Walker, and E.D. Salmon. 1997. A metastable intermediate state of microtubule dynamic instability that differs significantly between plus and minus ends. *J. Cell Biol.* 138:105–117. <https://doi.org/10.1083/jcb.138.1.105>
- Tropini, C., E.A. Roth, M. Zanic, M.K. Gardner, and J. Howard. 2012. Islands containing slowly hydrolyzable GTP analogs promote microtubule rescues. *PLoS One*. 7:e30103. <https://doi.org/10.1371/journal.pone.0030103>
- van den Berg, C.M., V.A. Volkov, S. Schnorrenberg, Z. Huang, K.E. Stecker, I. Grigoriev, S. Gilani, K.M. Frikstad, S. Patzke, T. Zimmermann, et al. 2023. CSPPI stabilizes growing microtubule ends and damaged lattices from the luminal side. *J. Cell Biol.* 222:e202208062. <https://doi.org/10.1083/jcb.202208062>

- Vemu, A., E. Szczesna, E.A. Zehr, J.O. Spector, N. Grigorieff, A.M. Deaconescu, and A. Roll-Mecak. 2018. Severing enzymes amplify microtubule arrays through lattice GTP-tubulin incorporation. *Science*. 361: 768. <https://doi.org/10.1126/science.aau1504>
- Voter, W.A., E.T. O'Brien, and H.P. Erickson. 1991. Dilution-induced disassembly of microtubules: Relation to dynamic instability and the GTP cap. *Cell Motil. Cytoskeleton*. 18:55–62. <https://doi.org/10.1002/cm.970180106>
- Walker, R.A., N.K. Pryer, and E.D. Salmon. 1991. Dilution of individual microtubules observed in real time in vitro: Evidence that cap size is small and independent of elongation rate. *J. Cell Biol.* 114:73–81. <https://doi.org/10.1083/jcb.114.1.73>
- Wasilko, D., and S.E. Lee. 2006. TIPS: Titerless infected-cells preservation and scale-up. *BioProcess J.* 5:29–32. <https://doi.org/10.12665/J53.WasilkoLee>
- Wasilko, D.J., S.E. Lee, K.J. Stutzman-Engwall, B.A. Reitz, T.L. Emmons, K.J. Mathis, M.J. Bienkowski, A.G. Tomasselli, and H.D. Fischer. 2009. The titerless infected-cells preservation and scale-up (TIPS) method for large-scale production of NO-sensitive human soluble guanylate cyclase (sGC) from insect cells infected with recombinant baculovirus. *Protein Expr. Purif.* 65:122–132. <https://doi.org/10.1016/j.pep.2009.01.002>
- Ye, X., T. Kim, E.A. Geyer, and L.M. Rice. 2020. Insights into allosteric control of microtubule dynamics from a buried β -tubulin mutation that causes faster growth and slower shrinkage. *Protein Sci.* 29:1429–1439. <https://doi.org/10.1002/pro.3842>
- Yu, N., L. Signorile, S. Basu, S. Ottema, J.H.G. Lebbink, K. Leslie, I. Smal, D. Dekkers, J. Demmers, and N. Galjart. 2016. Isolation of functional tubulin dimers and of tubulin-associated proteins from mammalian cells. *Curr. Biol.* 26:1728–1736. <https://doi.org/10.1016/j.cub.2016.04.069>

Supplemental material

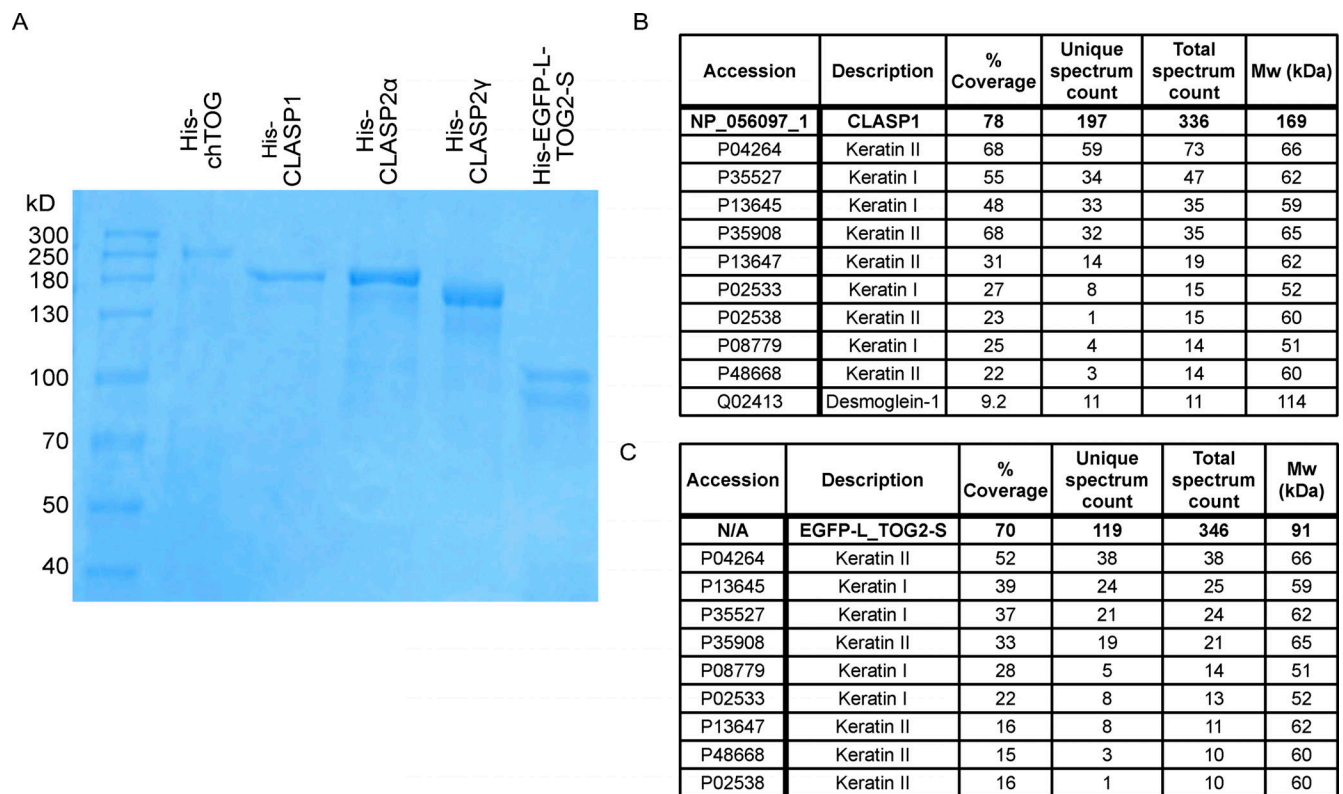


Figure S1. **Purification of proteins used in this study.** (A) SDS-page gel showing purified His-chTOG, His-CLASP1, His-CLASP2 α , His-CLASP2 γ , and His-EGFP-L-TOG2-S proteins. The lower band in the His-EGFP-L-TOG2-S sample likely represents a truncated protein or breakdown product as no significant contaminating proteins were found in the mass spectrometry analysis. (B) Mass spectrometry analysis of His-CLASP1 protein. (C) Mass spectrometry analysis of His-EGFP-L-TOG2-S protein. The hits with a total spectrum count of 10 or more are listed. Source data are available for this figure: SourceData FS1.

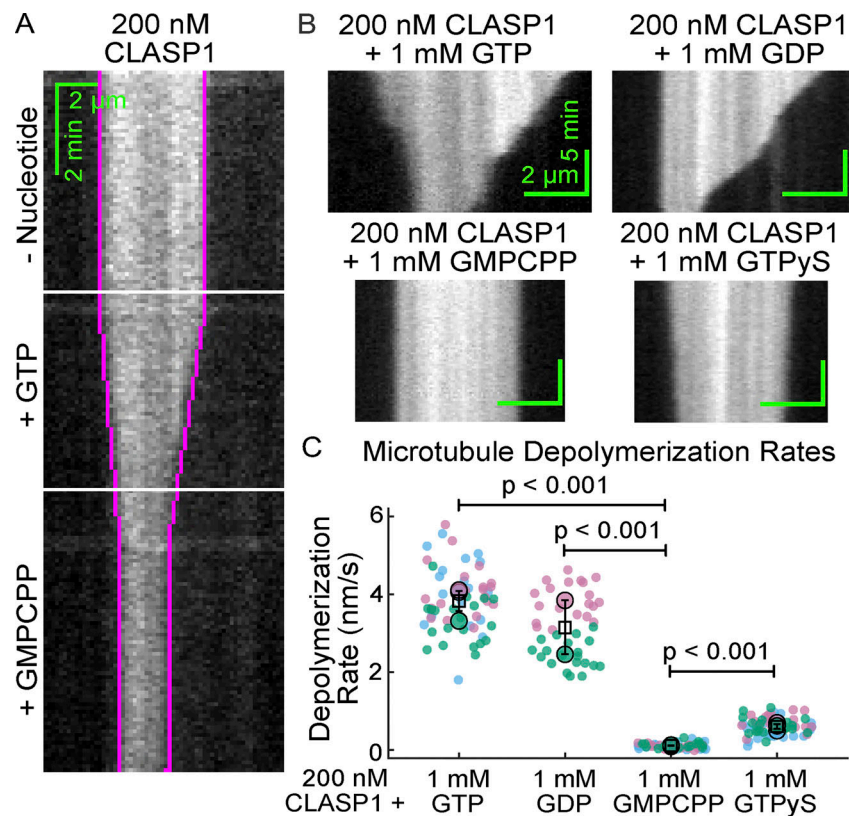


Figure S2. **The post-hydrolysis nucleotide state is required for CLASP1-mediated microtubule depolymerization.** **(A)** Representative kymograph of a GMPCPP-stabilized microtubule incubated sequentially with no nucleotide, 1 mM GTP, and 1 mM GMPCPP. The white horizontal lines indicate the times of solution exchange; the purple line is a manual trace of the microtubule end position overlaid onto the kymograph. **(B)** Representative kymographs of GMPCPP-stabilized microtubules incubated with buffer or 200 nM CLASP1 in the presence of 1 mM GDP, 1 mM GMPCPP, and 1 mM GTPyS. **(C)** Quantification of microtubule depolymerization rates for the conditions in the presence of different nucleotides. The mean depolymerization rates were 3.8 ± 0.3 nm/s; (SE, $N = 60$) with GTP, 3.1 ± 0.7 nm/s; (SE, $N = 40$) with GDP, 0.115 ± 0.008 nm/s; (SE, $N = 60$) with GMPCPP, and 0.61 ± 0.06 nm/s; (SE, $N = 60$) with GTPyS. Data were obtained from at least two independent experimental days and individual data points from different experiments are plotted in different shades. The means for each experimental repeat are plotted as larger points in the same color. The squares indicate the average of the experimental means, and the vertical bars are the standard errors of the means. A one-way ANOVA followed by Tukey's HSD test for multiple comparisons revealed that there was a statistically significant difference in the microtubule depolymerization rate between GTP and GMPCPP ($P < 0.001$), GDP and GMPCPP ($P < 0.001$), and GTPyS and GMPCPP ($P < 0.001$). The corresponding P values are also indicated on the graph.

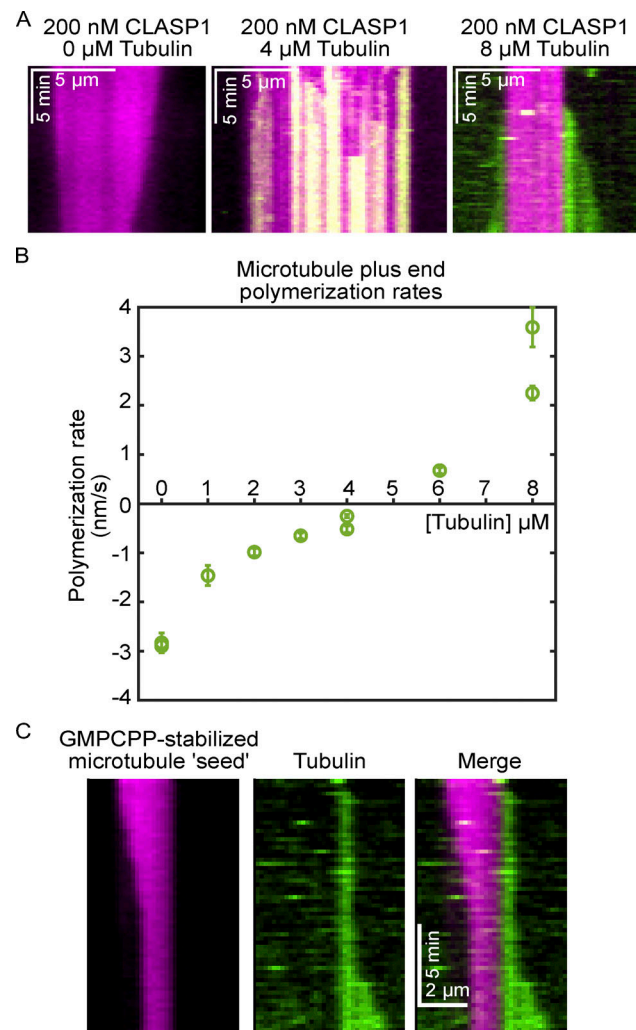


Figure S3. **Soluble tubulin does not abolish CLASP's depolymerase activity until the tubulin concentration is above the critical concentration for microtubule growth.** **(A)** Representative kymographs of microtubules in the presence of 0, 4 and 8 μ M soluble tubulin and 200 nM CLASP1. The stable microtubule seed is shown in magenta and the tubulin is shown in green. **(B)** Quantification of the microtubule plus-end polymerization rate across a range of tubulin concentrations from 0 to 8 μ M in the presence of 200 nM CLASP1. Data are means \pm SE obtained over three experimental days. **(C)** An example kymograph of a microtubule undergoing CLASP-mediated depolymerization at one end and polymerization at the other in the presence of 8 μ M soluble tubulin and 200 nM CLASP1.

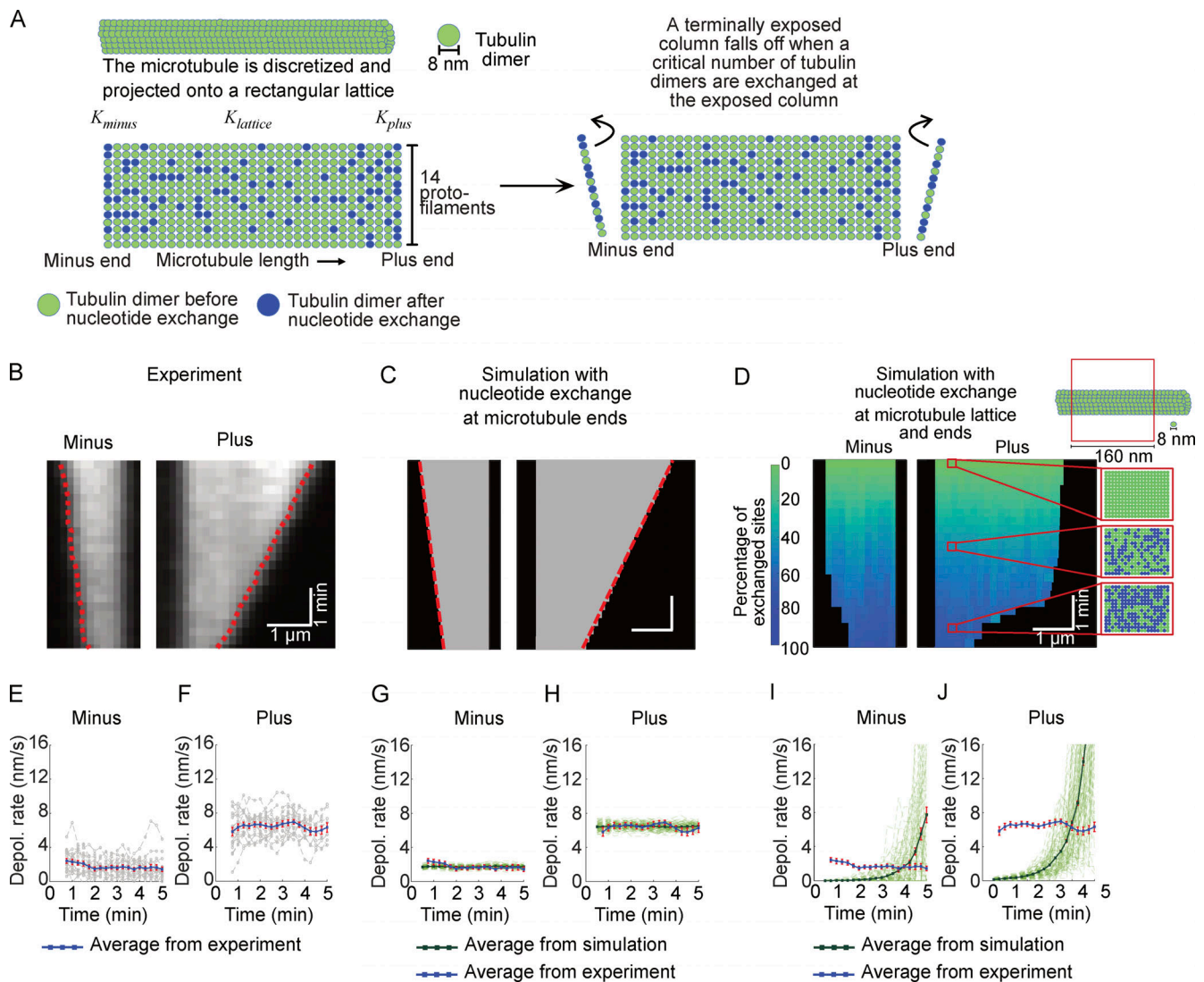


Figure S4. **Computational modeling demonstrates that nucleotide exchange in the microtubule lattice does not recapitulate the characteristics of the microtubule depolymerization observed in experiments.** (A) Schematics of the computational model for CLASP-dependent nucleotide exchange leading to depolymerization. See Table S2 for a list of the model parameters. (B) A representative kymograph of an experimental microtubule depolymerizing in the presence of 1 mM GTP and 61.5 nM CLASP. The red dashed lines indicate the traces of the microtubule ends obtained using KymographClear and KymographDirect (Mangeol et al., 2016). (C) A representative kymograph of microtubule depolymerization simulated using the model of nucleotide exchange solely at the microtubule ends. (D) A representative kymograph of microtubule depolymerization simulated using model of nucleotide exchange throughout the entire microtubule lattice in addition to the exchange at the ends. The color map represents the percentage of exchanged sites on the microtubule. The “zoomed in” regions on the kymograph show the tubulin dimers within a 160 nm long segment on the microtubule lattice at three different time points (0, 2.5 and 5 min). Over the course of time, more and more tubulin dimers are exchanged (“green” sites turning into “blue” sites) within the microtubule lattice. (E and F) The time dependence of depolymerization rate at microtubule minus (E) and plus (F) ends as observed in experiments. In E and F, the gray curves denote trajectories obtained from individual microtubules in experiment ($N = 20$). The blue curve denotes the average curve evaluated from gray trajectories. (G and H) The time dependence of depolymerization rate at microtubule minus (G) and plus (H) ends as obtained from the model of nucleotide exchange solely at the microtubule ends. (I and J) The time dependence of depolymerization rate at microtubule minus (I) and plus (J) ends as obtained from the model of nucleotide exchange throughout the entire microtubule lattice in addition to the exchange at the ends. In G–J, the light green curves denote trajectories obtained from individual microtubules in simulation. The dark green curve denotes the average curve evaluated from individual microtubule trajectories in simulation. The instantaneous depolymerization rates presented in E–J were estimated by averaging over a 1-min time window. The error bars represent SEM ($N = 20$ in experiment, $N = 100$ in all simulated cases).

Video 1. **GMPCPP-stabilized microtubules (shown in gray) were incubated with 200 nM CLASP1 in the absence (left) and presence of 1 mM GTP (right) and imaged by TIRF microscopy.** Time is shown in min:s. Images were taken every 15 s, and the video playback is 10 fps. Related to Fig. 1.

Video 2. **Polarity-marked, GMPCPP-stabilized microtubules were incubated with 1 mM GTP in the absence (left) or presence of 500 nM CLASP1 (right) and imaged by TIRF microscopy.** The GMPCPP-stabilized microtubule “seed” is shown in magenta, and the GMPCPP-stabilized microtubule extensions are shown in green. The longer extension is the plus end and the shorter extension is the minus end. Time is shown in min:s. Images were taken every 15 s and the video playback is 20 fps. Related to [Fig. 5](#).

Provided online are Data S1, Table S1, and Table S2. Data S1 contains the data underlying Figs. 1–5 and Figs. S2 and S3. Table S1 shows depolymerization rates of different microtubule substrates in the presence and absence of CLASP1. Table S2 lists model parameters. Related to Fig. S4.